WAVE LOCALIZATION AND MULTIPLE SCATTERING IN RANDOMLY-LAYERED MEDIA

PING SHENG, BENJAMIN WHITE, ZHAO-QING ZHANG*
Exxon Research and Engineering Company, Route 22 East
Clinton Township, Annandale, NJ 08801
and
GEORGE PAPANICOLAOU
Courant Institute of Mathematical Sciences
New York University, New York, NY 10012

We present a tutorial review of the theoretical developments in the calculation of localization length and pulse backscattering statistics for a randomly-layered medium. By using the approach of stochastic differential equations, it is shown that the localization length $l(\omega) \sim \omega^{-2}$ at low frequencies and is non-decreasing at high frequencies. Analytical expressions for $l(\omega)$ in the two limits are compared with numerical simulation results for three different types of layered models. Excellent agreement is obtained. Furthermore, for oblique-incident electromagnetic waves it is found that the localization length for one of the

* *Present address:* Institute of Physics, Academia Sinica, Beijing, People's Republic of China.

polarizations can increase by orders of magnitude (and sometimes diverges) at a particular angle, a phenomenon that may be directly related to the Brewster effect for reflection from a plane interface. For pulse backscattering from a randomly stratified halfspace, the calculation of the power spectrum S for the multiply-backscattered signal train is formulated in terms of the correlation of the reflection coefficients at two different frequencies. Analytical solution of this correlation function in the white-noise limit (correlation length of the material parameter fluctuations$\rightarrow$ 0) gives the result that $S = |f(\omega)|^2 \mu(\chi)/\tau$, where $\chi =$ (distance traveled by the pulse at time τ)/(the frequency-dependent localization length $l(\omega)$), $f(\omega)$ is the pulse frequency spectrum, and $\mu = \chi/(1+\chi)^2$ and 4χ for the matched-impedance and total-reflection boundary conditions at the halfspace interface, respectively. Numerical simulations give excellent support to the analytical results even for model parameter values much beyond the white noise regime. We offer a plausible explanation for the robust nature of the analytical solution and discuss its physical implications for the time-domain measurement of $l(\omega)$.

Contents

1. Introduction 566

2. Statement of Results 567

3. Model Description 569

4. Localization Length of a Randomly-Layered Medium 572
   - 4.1. Stochastic differential equation approach to the calculation of $l(\omega)$ 572
   - 4.2. Low frequency solution 575
   - 4.3. High frequency solution 582
   - 4.4. Oblique incidence 586
   - 4.5. Numerical simulations 590

5. Localization Characteristics in the Time Domain 599
   - 5.1. Formulation 599
   - 5.2. Solution in the white noise limit 603
   - 5.3. Numerical simulations 611
   - 5.4. Physical implications 616

6. Concluding Remarks 617

Appendix 618

References 619

1. INTRODUCTION

The study of wave propagation and scattering in randomly-layered media has long been a subject of active interest. As a reasonable approximation to earth's stratified lithology, the layered-medium model is basic to the geophysical calculations involving forward modeling and inversion of seismic data.[1] The simplicity of the layered geometry, on the other hand, also offers a convenient setup for working out the physics of localization phenomenon.[2] In recent years, significant progress has been made in clarifying the statistical character of the multiply-scattered wave in a randomly-layered medium.[3-15] In particular, it was found that besides the usual localization behavior for the single-frequency wave in the form of exponential decay with a frequency-dependent decay (localization) length $l(\omega)$, there are additional generic time-domain characteristics associated with the scattering and localization of a pulse.[3-5] Since the concept of time-domain localization is relatively new but yet important for many applications, below we describe in more detail both the phenomenon and its potential implications.

There are many industrial and geophysical examples where the probing of a medium is accomplished not by continuous harmonic waves but rather by transient pulses. In these cases the medium response is in the form of a time trace for the backscattered or transmitted signals. When the medium is random, these time-dependent signals are generally characterized by the presence of a long noisy tail, known as coda, arising from multiple scattering of the pulse. A good example of this can be found in the coda following the arrival of each seismic pulse after it has traversed the inhomogeneous earth.[7] While the structure of this tail follows deterministically from the structure and properties of the earth, the possibility of recovering this type of detailed information from the coda is nevertheless rather remote since the information is thoroughly scrambled by multiple scattering. Two relevant questions are then: (1) What information, if any, can be extracted from this type of noise? (2) Is there a generic localization characteristic in the time-domain response to a transient pulse?

It is the purpose of the present chapter to review the recent theoretical progress in the understanding of wave and pulse localization in

randomly-layered media. In order to have an overall picture of what follows, we will first summarize the key results as well as answer the two questions posed above before delving into more detailed developments.

2. STATEMENT OF RESULTS

Except for polarization-induced effects in vector waves,[9] it is well-known that all waves localize in a randomly-stratified medium when the propagation direction is normal to the layers. The relevant question is therefore the value of the localization length and its frequency dependence. At low frequencies, where the wavelength λ far exceeds the correlation length of the inhomogeneities, the wave essentially "sees" a nearly homogeneous effective medium and the localization length $l(\omega)$ can be shown to diverge as $\gamma_1^{-1}\omega^{-2}$. The proportionality constant, γ_1^{-1}, is particular to the medium and is dependent on the integral of the correlation function for the random material parameters.[6] At high frequencies, it can be shown that $l(\omega)$ is non-decreasing.[6] For a model with sharp inter-layer boundaries, $l(\omega)$ saturates to a constant c_1^{-1}. But since at high frequencies the wave can resolve the details of the inhomogeneities, the value of c_1 is dependent on the nature of the interfaces. In particular, for models with continuous variation of the material parameters (or fuzzy interfaces betweeen layers) $c_1 = 0$ and $l(\omega)$ diverges[6] as $\omega \to \infty$. However, as long as there is an interface region, then for wavelength larger than the interface region $l(\omega)$ may be accurately described by the interpolation relation

$$l(\omega) = c_1^{-1} + \frac{1}{\gamma_1 \omega^2} \ . \tag{1}$$

Besides their model dependence, the parameters c_1 and γ_1 can also vary as a function of the angle of incidence θ. A striking example may be found in the case of the electromagnetic wave when the transverse magnetic field vector is polarized parallel to the layerings and perpendicular to the plane of incidence. The localization length is found to increase by orders of magnitude at a particular angle of propagation, an effect directly traceable to the well-known Brewster effect for reflection from a plane interface.

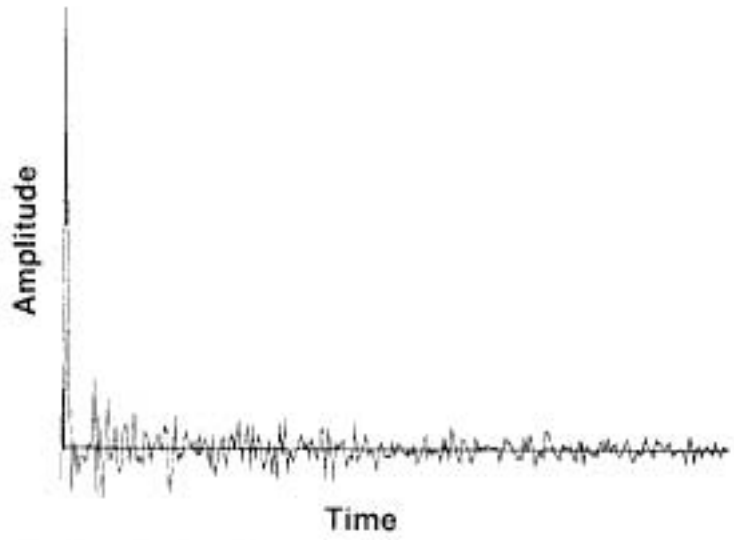

Fig. 1. Numerically simulated time-dependent response to a pressure pulse incident on a randomly-layered halfspace. The observer is at the interface between the homogeneous medium and the randomly-layered medium.

In the case of a pulse, the localization behavior has to be described in quite different terms. Figure 1 shows the numerically calculated response, at the interface between a randomly-layered halfspace and a homogeneous halfspace, resulting from an incident (plane-wave) pulse. It is seen that the initial injection of the pulse is followed by a long tail arising from multiply-backscattered wave field. The time series is obviously non-stationary in the sense that the statistics of both the magnitude and the frequency content of the signal changes with time. That means if one calculates the power spectrum S of the noisy tail, then S is not only a function of the frequency ω, but also depends on the choice of the time window in which the frequency spectrum is calculated, i.e. $S = S(\tau, \omega)$, where τ denotes the center of the time window. Our analytical and numerical simulation[3-5] results indicate that for an incident pulse with frequency spectrum $f(\omega), S(\tau, \omega) = |f(\omega)|^2 \tau^{-1} \mu(\chi)$, where μ is an universal function independent of material parameters, $\chi = \tau v_0 / l(\omega)$, v_0 is the effective-medium speed of the medium, and $l(\omega)$ is the frequency-dependent localization length. We have also determined the explicit forms of μ as $\chi/(1+\chi)^2$ and 4χ, for the transmitting and the reflecting boundary conditions at the halfspace interface, respectively. The existence of a universal function independent of the

statistics of the model as well as its material parameters clearly indicates that the power spectrum has a generic character which is a signature of the localization effect in the time domain. This fact therefore answers one of the questions posed earlier. As to the other question regarding the information extractable from back-scattered coda, we note that since $l(\omega)$ is the only quantity in $S(\tau,\omega)$ that is particular to the medium, it thus represents the maximum statistical information obtainable. The power spectrum function is therefore the composition of a generic function μ with a material-dependent function $l^{-1}(\omega)$. Prior knowledge of both functions would open the possibility for constructing statistical filters for enhancing signals, i.e. scattering from target objects embedded in a random medium, through multiple-scattering noise suppression.

In what ensues, the results described above and their implications will be developed in more detail. Description of the three different types of layered models is given in Sec. 3. This is followed by the consideration of the frequency dependence of the localization length $l(\omega)$ in Sec. 4. The pulse backscattering problem and its physical implications are addressed in Sec. 5, and Sec. 6 concludes with a discussion of further topics.

3. MODEL DESCRIPTION

Consider a randomly-layered halfspace in the region $0 \leq z < \infty$ characterized by spatially varying density $\rho(z)$, elastic bulk modulus $K(z)$, dielectric constant $\varepsilon(z)$, and magnetic permeability $\mu(z)$. The elastic wave equation is given by

$$\rho\dot{w} = -\frac{\partial p}{\partial z}\,, \tag{2a}$$

$$\dot{p} = -K\frac{\partial w}{\partial z}\,, \tag{2b}$$

where w is the displacement velocity, p the pressure, and the over-dot denotes time derivative. The equation for electromagnetic wave propagation normal to the layering direction can be obtained from Eq. (2) by making the following substitutions: $\varepsilon/c \to \rho, c/\mu \to K$, transverse

electric field $\rightarrow w$, transverse magnetic field $\rightarrow p$. Here c denotes the speed of light in vacuum. Since the two equations are identical under the transformation, the results obtained in one case are assured to be applicable in the other case as well. In this article we will use the acoustic notations except for the discussion of oblique incidence in Sec. 4.4, where the electromagnetic case differs from the acoustic one.

The random quantities in Eq. (2) are $\rho(z)$ and $K(z)$, the materials parameters. We consider three types of random models. In model I, $\rho(z)$ and $K(z)$ are piecewise constant in layers of equal thickness $\overline{a}$:

$$\rho_i = \rho_0[1 + 2\sigma_\rho \xi_1(z)] \,, \tag{3a}$$

$$K_j^{-1} = K_0^{-1}[1 + 2\sigma_K \xi_2(z)] \,, \tag{3b}$$

where i (or j) denotes the ith (or jth) layer, ξ_1, ξ_2 are random step functions which jump simultaneously at layer interfaces and whose values are independent and uniformly distributed in the interval $[-\frac{1}{2}, \frac{1}{2}]$, and $0 \leq \sigma_{\rho(K)} < 1$ specifies the amount of randomness as a fraction of the mean. In model II, $\rho(z)$ and $K(z)$ have the same piecewise-constant profiles as given by Eq. (3), but the layer thickness a is now a random variable with an exponential distribution $\exp(-a/\overline{a})/\overline{a}$, where $\overline{a}$ denotes the mean layer thickness. Model III differs from the first two in that $\rho(z)$ and $K(z)$ are continuous functions of z. More precisely, if we let $\overline{m}_i$ denote the material parameter ρ or K^{-1} of model II and m_i denotes that of model III, then

$$\frac{dm_i(z)}{dz} = \overline{m}_i(z) - m(z) \,, \tag{4a}$$

or

$$m_i(z) = \exp(-z) \otimes \overline{m}(z) = \exp(z_1 - z) m_i(z_1) + [1 - \exp(z_1 - z)]\overline{m}_i \,, \tag{4b}$$

where $z_1 < z$ denotes the coordinate for the lower end of the layer, and the symbol $\otimes$ denotes convolution. The three models are schematically depicted in Fig. 2.

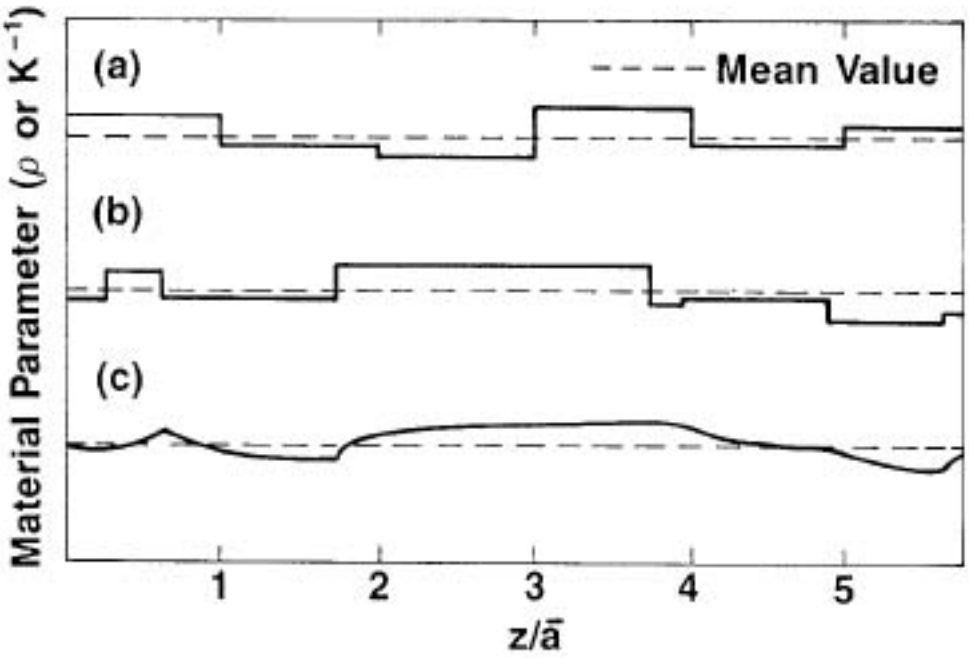

Fig. 2. Three types of randomly-layered models. (a) Model I has equal layer thickness and random material properties from one layer to the next. (b) Model II has variable layer thickness with an exponential distribution as well as random material properties from layer to layer. (c) Model III has continuous but random variation of the material properties.

While for the localization length calculation the boundary condition at $z = 0$ does not matter since $l(\omega)$ is an intrinsic property of the random medium, for the pulse reflection problem the form of the power spectrum function does depend on whether the interface at $z = 0$ is transmitting or reflecting. We will consider two choices for the region $-\infty < z \leq 0$. The first one is a homogeneous medium with $\rho = \rho_0, K = K_0$, and mean velocity $v_0 = (K_0/\rho_0)^{\frac{1}{2}}$. In this case the mean impedance of the two half-spaces are matched in the effective-medium sense so that the boundary at $z = 0$ is transmitting to the pulse. This is denoted as the matched-medium boundary condition. The second choice is for the random medium to border a vacuum so that the interface is totally reflecting to the backscattered wave. This is denoted as the reflecting boundary condition. Effects arising from the different boundary conditions will be addressed in Sec. 5.

4. LOCALIZATION LENGTH OF A RANDOMLY-LAYERED MEDIA

4.1. Stochastic Differential Equation Approach to the Calculation of $l(\omega)$

We start by rewriting Eq. (2) in the frequency domain, letting $\exp(-i\omega t)$ be the time dependence of w and p:

$$\frac{d}{dz}\begin{pmatrix} p \\ u \end{pmatrix} = \omega \begin{bmatrix} 0 & \rho(z) \\ -K^{-1}(z) & 0 \end{bmatrix} \begin{pmatrix} p \\ u \end{pmatrix} , \tag{5}$$

where $u = iw$ is defined so that Eq. (5) is completely real. Localization means that as $z \to \infty$, the envelope describing the magnitude of the physical solution (p, u) must decay as $\exp(-\gamma z)$, where $\gamma = l^{-1}(\omega)$. Since Eq. (5) represents two coupled first-order differential equations, there must be a second independent solution. Due to the fact that the 2×2 matrix in Eq. (5) has zero trace, it may be simply demonstrated (see Appendix) that the second solution must exhibit an exponentially growing behavior, $\exp(\gamma z)$, with exactly the same γ. For a set of arbitrary initial conditions (not necessarily physical) at $z = 0$, the solution to Eq. (5) is expressible as the sum of two linearly independent solutions. Provided that the coefficient of the exponentially growing solution is not identically zero, it will always dominate in the $z \to \infty$ limit. Our strategy for calculating γ is therefore to choose a set of convenient, arbitrary initial conditions and then to calculate γ for random realizations of $\rho(z), K^{-1}(z)$ by measuring the rate of their exponential growth. To implement this, we would like to first make a polar-coordinate transformation defined by $p = r\cos\phi$, $u = r\sin\phi$ so that the magnitude information may be inferred from r alone. The new equations take the form

$$\frac{d\phi}{dz} = -\omega[\rho(z)\sin^2\phi + K^{-1}(z)\cos^2\phi] , \tag{6a}$$

$$\frac{dr}{dz} = (r\omega/2)\sin 2\phi[\rho(z) - K^{-1}(z)] . \tag{6b}$$

The ϕ equation now is noted to be decoupled from the r equation, which can therefore be integrated to obtain

$$\ln\left(\frac{r}{r_0}\right) = \frac{\omega}{2}\int_0^z \sin 2\phi\{\rho[\xi_1(z)] - K^{-1}[\xi_2(z)]\}dz , \tag{7}$$

where $r_0 = r(z=0)$. Since it is expected that $\ln r \simeq \ln$ (constant) $+\gamma z$ as $z \to \infty$, that means

$$\lim_{z\to\infty} \frac{\ln r}{z} = \gamma = \frac{\omega}{2} \left\{ \lim_{z\to\infty} \frac{1}{z} \int_0^z \sin 2\phi \{\rho[\xi_1(z')] - K^{-1}[\xi_2(z')]\} dz' \right\} . \tag{8}$$

We recognize from Eq. (8) that γ is essentially $\omega/2$ times the spatial average of $\sin 2\phi[\rho - K^{-1}]$ in the limit of $z \to \infty$. If the joint stationary distribution function $P(\phi, \xi_1, \xi_2)$ is known, then the spatial averaging that appears in Eq. (8) can be rewritten as

$$\gamma = \frac{\omega}{2} \int_0^{2\pi} d\phi \iint_{-\frac{1}{2}}^{\frac{1}{2}} d\xi_1 d\xi_2 P(\phi, \xi_1, \xi_2) \sin 2\phi[\rho(\xi_1) - K^{-1}(\xi_2)] . \tag{9}$$

To determine P, we just note that if (ϕ, ξ_1, ξ_2) represents a Markov process, then P must satisfy the stationary Fokker-Planck equation

$$L^* P(\phi, \xi_1, \xi_2) = 0 , \tag{10a}$$

where

$$L = Q + \frac{d\phi}{dz} \frac{d}{d\phi} , \tag{10b}$$

L^* is the adjoint of L, and Q is the infinitesimal generator associated with the random jump processes ξ_1 and ξ_2. Since the operator Q underlies many of the calculations in the rest of this work, we wish to make a little digression here in order to define it more concretely in terms of the three random material models.

A infinitesimal generator is defined as the operation of taking the stochastic derivative[16]:

$$Qf(\xi_0) = \lim_{\Delta z\to 0} (\Delta z)^{-1} \{E[f(\xi(\Delta z))|\xi(0) = \xi_0] - f(\xi_0)\} , \tag{11}$$

where the notation $E[\ ]$ denotes the operation of taking the expectation value. The knowledge of Q directly generates the dynamical equation $\partial u/\partial z = Qu$ (also known as the backward Kolmogorov equation). For Markovian processes ξ_1 and ξ_2, such as Model II, we can calculate $Qf(\xi_1, \xi_2)$ as follows. Since ξ_1 and ξ_2 jump simultaneously,

the probability density of no jump in an increment Δz is given by $\exp(-\Delta z/\bar{a})$, where $\bar{a}$ is the mean separation between two consecutive jumps. The expectation value is therefore the probability density of no jump ($\exp(-\Delta z/\bar{a})$) times $f(\xi_1^{(0)}, \xi_2^{(0)})$, plus the probability density of a jump, $1-\exp(-\Delta z/\bar{a})$, times the integral of $f(\xi_2, \xi_2)$ over the square $[-\frac{1}{2}, \frac{1}{2}] \times [-\frac{1}{2}, \frac{1}{2}]$ since once the jump occurs, ξ_1 and ξ_2 can take any new value within the square. In short,

$$\begin{aligned} Qf(\xi_1^{(0)}, \xi_2^{(0)}) &= \lim_{\Delta z \to 0} (\Delta z)^{-1} \{E[f(\xi_1(\Delta z), \xi_2(\Delta z)) | \xi_1(0) = \xi_1^{(0)}, \\ &\qquad \xi_2(0) = \xi_2^{(0)}] - f(\xi_1^{(0)}, \xi_2^{(0)})\} \\ &= \lim_{\Delta z \to 0} (\Delta z)^{-1} \{\exp(-\Delta z/\bar{a}) f(\xi_1^{(0)}, \xi_2^{(0)}) \\ &\qquad + [1 - \exp(-\Delta z/\bar{a})] \iint_{-\frac{1}{2}}^{\frac{1}{2}} d\xi_1 d\xi_2 f(\xi_1, \xi_2) \\ &\qquad - f(\xi_1^{(0)}, \xi_2^{(0)})\} \\ &= (\bar{a})^{-1} \int_{-\frac{1}{2}}^{\frac{1}{2}} d\xi_1 \int_{-\frac{1}{2}}^{\frac{1}{2}} d\xi_2 [f(\xi_1, \xi_2) - f(\xi_1^{(0)}, \xi_2^{(0)})] . \end{aligned} \tag{12a}$$

If we let $\overline{P}(\xi_1, \xi_2) = 1$ denote the stationary distribution of (ξ_1, ξ_2), it is clear that $Q^* \overline{P} = 0$, i.e. $\overline{P}$ satisfies the stationary Fokker-Planck equation for (ξ_1, ξ_2). In other words, $\overline{P}$ constitutes the null space of Q^*.

When (ξ_1, ξ_2) represents jumps at equally-spaced intervals as that in model I, the process is only discretely Markovian, and the formalism based on continuous Markov process as described above is not applicable in the strict sense. However, we will argue on physical grounds that the results obtained at high and low frequencies may still pertain, provided we make certain assumptions. Quantitative results thus obtained are verified by numerical simulations. However, in the intermediate frequency range model I does differ significantly from model II as will be seen in Sec. 4.5.

For model III, the generators of the Markov process are the ξ_i's plus the η_i's, defined by

$$\frac{d\eta_i}{dz} = (\xi_i - \eta_i), \quad i = 1, 2$$

as specified by Eq. (4a), where $\rho = \rho_0(1+2\sigma_\rho\eta_1)$ and $K^{-1} = K_0^{-1}(1+2\sigma_K\eta_2)$ are the material parameters of model III. The infinitesimal generator Q is therefore

$$\begin{aligned} Q &= Q_\epsilon + \frac{d\eta_1}{dz}\frac{\partial}{\partial\eta_1} + \frac{d\eta_2}{dz}\frac{\partial}{\partial\eta_2} \\ &= Q_\epsilon + (\xi_1-\eta_1)\frac{\partial}{\partial\eta_1} + (\xi_2-\eta_2)\frac{\partial}{\partial\eta_2}\ , \end{aligned} \tag{12b}$$

where Q_ϵ denotes that given by Eq. (12a). In what follows, formal considerations will only be given to the case of model II, where $Q = Q_\epsilon$. The η_i's will be noted only in regard to their effect on the final results for model III.

Now back to Eq. (10b), we see that by using Eq. (6a) for $(d\phi/dz)$, the operator L may be written as

$$L = Q - \omega(\rho\sin^2\phi + K^{-1}\cos^2\phi)\frac{\partial}{\partial\phi}\ , \tag{13}$$

and the stationary Fokker-Planck equation for $P(\phi,\xi_1,\xi_2)$ is

$$Q^*P + \omega\frac{\partial}{\partial\phi}[(\rho\sin^2\phi + K^{-1}\cos^2\phi)P] = 0\ . \tag{14}$$

At present, no general solution of Eq. (14) is known. Below we present solutions of Eq. (14) in both the low- and the high-frequency limits and thereby get the behavior of the localization length in these regimes.

4.2. Low Frequency Solution

By assuming ω to be a small parameter, we expand P as

$$P = P^{(0)} + \omega P^{(1)} + \omega^2 P^{(2)} + \dots \tag{15}$$

From Eq. (9) that means $\gamma = \gamma_0\omega + \gamma_1\omega^2 + \dots$, where γ_n is determined by the respective $P^{(n)}$. Denoting the quantity $(\rho\sin^2\phi + K^{-1}\cos^2\phi)$ as F, we get from Eqs. (14) and (15)

$$Q^*P^{(0)} + \omega Q^*P^{(1)} + \omega^2 Q^*P^{(2)} + \dots = -\omega\frac{\partial}{\partial\phi}FP^{(0)} - \omega^2\frac{\partial}{\partial\phi}FP^{(1)}\dots\ , \tag{16a}$$

or, by equating terms with the same power of ω,

$$Q^* P^{(0)} = 0 \,, \tag{16b}$$

and

$$Q^* P^{(n)} + \frac{\partial}{\partial \phi} F P^{(n-1)} = 0; \quad n \geq 1 \,. \tag{16c}$$

Starting with $P^{(0)}$, we see from Eq. (16b) that $P^{(0)}$ must be proportional to the null space vector of Q^*, i.e.

$$P^{(0)} = \overline{P}(\xi_1, \xi_2) g_0(\phi) \,. \tag{17}$$

In order to get the form of $g_0(\phi)$, let us consider the next order equation

$$Q^* P^{(1)} = -\frac{\partial}{\partial \phi} F P^{(0)} \,. \tag{18}$$

Since Q^* has a non-trivial null-space, it is a singular operator and Eq. (18) will be solvable only if its right-hand side, $-\frac{\partial}{\partial \phi} F P^{(0)}$, is orthogonal to the null space of Q^*. This is so because otherwise $(Q^*)^{-1}$ would not be well-defined. The so-called "solvability condition" means that

$$\int d\boldsymbol{\xi} \frac{\partial}{\partial \phi} F P^{(0)} = 0 \,, \tag{19}$$

(here and in the rest of this work the region of integration for $\int d\boldsymbol{\xi}$ will be understood to be square $[-\frac{1}{2}, \frac{1}{2}] \times [-\frac{1}{2}, \frac{1}{2}]$) because the integration with respect to the left-hand side of Eq. (18) yields

$$\int Q^* P^{(1)} d\boldsymbol{\xi} = \int P^{(1)} Q \cdot 1 d\boldsymbol{\xi} = 0 \,,$$

i.e. integrate with respect to $\boldsymbol{\xi} = (\xi_1, \xi_2)$ is equivalent to taking the inner product with the null-space vector $\overline{P} = 1$. Substitution of Eq. (17) into Eq. (19) gives

$$\frac{\partial}{\partial \phi} \overline{F} g_0(\phi) = 0 \,, \tag{20a}$$

where

$$\overline{F} = \rho_0 \sin^2 \phi + K_0^{-1} \cos^2 \phi \tag{20b}$$

is obtained by averaging F with respect to $\boldsymbol{\xi}$ (integrating F with $\overline{P}$). Equation (20a) gives the solution of

$$g_0(\phi) = \frac{(\text{const.})}{\overline{F}} \ . \tag{21a}$$

By requiring the normalization conditions that $g_0(\phi)$ must integrate to 1, we get const. $= (2\pi v_0)^{-1}$ with $v_0 = \sqrt{K_0/\rho_0}$. Therefore,

$$P^{(0)}(\phi, \xi_1, \xi_2) = \frac{1}{2\pi v_0} \frac{\overline{P}(\xi_1, \xi_1)}{\rho_0 \sin^2\phi + K_0^{-1}\cos^2\phi} \tag{22}$$

is the solution for $P(\phi, \xi_1, \xi_2)$ to the leading order. With the knowledge of $P^{(0)}$ we can now calculate, via Eq. (9), the inverse localization length $\gamma = \gamma_0\omega$ to the leading order:

$$\begin{aligned}\gamma_0 &= \frac{1}{2}\int_0^{2\pi} d\phi \iint_{-\frac{1}{2}}^{\frac{1}{2}} d\xi_1 d\xi_2 P^{(0)}(\phi, \xi_1, \xi_2) \sin 2\phi [\rho(\xi_1) - K^{-1}(\xi_2)] \\ &= \frac{1}{4\pi v_0}(\rho_0 - K_0^{-1}) \int_0^{2\pi} d\phi \frac{\sin 2\phi}{\rho_0 \sin^2\phi + K_0^{-1}\cos^2\phi} \\ &= 0 \ .\end{aligned} \tag{23}$$

That is, $P^{(0)}$ gives zero contribution to γ. In order to get the leading-order finite contribution, we must therefore calculate $P^{(1)}(\phi, \xi_1, \xi_2)$.

Let us return to Eq. (18) but now write it in a slightly different form:

$$Q^* P^{(1)} = -\frac{\partial}{\partial\phi} F P^{(0)} = -\frac{\partial}{\partial\phi}\overline{F}P^{(0)} - \frac{\partial}{\partial\phi}\widehat{F}P^{(0)} \ , \tag{24a}$$

where we have expressed F as the sum of its mean and a fluctuating part $\widehat{F}$ defined as

$$\widehat{F} = \rho\widehat{\rho}_0 \sin^2\phi + K_0^{-1}\widehat{K}^{-1}\cos^2\phi \ ,$$

with $\widehat{\rho} = (\rho - \rho_0)/\rho_0 = 2\sigma_\rho \xi_1$ and $\widehat{K}^{-1} = (K^{-1} - K_0^{-1})/K_0^{-1} = 2\sigma_K \xi_2$ denoting the normalized fluctuation in ρ and K^{-1} as given by Eq. (3). Now from Eqs. (17) and (21a), we have $\partial\overline{F}P^{(0)}/\partial\phi = 0$. Therefore,

$$Q^* P^{(1)} = -\frac{\partial}{\partial\phi}\widehat{F}P^{(0)} \ . \tag{24b}$$

Since Q^* is a singular operation, we can formally write the solution $P^{(1)}$ as

$$P^{(1)} = -(Q^*)^{-1}\frac{\partial}{\partial\phi}\hat{F}P^{(0)} + \overline{P}(\xi_1,\xi_2)g_1(\phi)\ . \tag{25}$$

Here the notation $(Q^*)^{-1}$ means the generalized inverse of Q^* defined on the space of vectors that is orthogonal to the null space (the fact that $\partial\hat{F}P^{(0)}/\partial\phi$ is indeed orthogonal to the null space is guaranteed by the solvability condition for Eq. (18)). For the part of $P^{(1)}$ that is proportional to the null vector $\overline{P}(\xi_1,\xi_2)$, we have denoted the function of proportionality as $g_1(\phi)$. To get $g_1(\phi)$, we must use the solvability condition for the next order equation

$$Q^*P^{(2)} = -\frac{\partial}{\partial\phi}FP^{(1)}\ , \tag{26}$$

given by the condition

$$\int d\boldsymbol{\xi}\frac{\partial}{\partial\phi}FP^{(1)} = 0\ , \tag{27a}$$

or

$$\begin{aligned}\beta &= \int d\boldsymbol{\xi}FP^{(1)}\\ &= \int d\boldsymbol{\xi}\left\{(\overline{F}+\hat{F})\left[-(Q^*)^{-1}\frac{\partial}{\partial\phi}\hat{F}P^{(0)}\right] + F\overline{P}(\boldsymbol{\xi})g_1(\phi)\right\}\\ &= \overline{F}g_1(\phi) + \int d\boldsymbol{\xi}\left[-\hat{F}(Q^*)^{-1}\frac{\partial}{\partial\phi}\hat{F}P^{(0)}\right]\ .\end{aligned} \tag{27b}$$

Here β is to be determined by the normalization condition for $g_1(\phi)$. In Eq. (27b) we have used the fact that the integration of $\overline{F}$ with $(Q^*)^{-1}\partial\hat{F}P^{(0)}/\partial\phi$ gives zero since $\overline{F}$ is independent of $\boldsymbol{\xi}$, and $(Q^*)^{-1}\partial\hat{F}P^{(0)}/\partial\phi$ is orthogonal to $\overline{P}$. By the definition of adjoint operator, this last integral in Eq. (27b) may also be written as

$$\int d\boldsymbol{\xi}\Big(-\hat{F}(Q^*)^{-1}\frac{\partial}{\partial\phi}\hat{F}P^{(0)}\Big) = \int d\boldsymbol{\xi}\Big(-\frac{\overline{P}}{2\pi v_0}\frac{\partial}{\partial\phi}\frac{\hat{F}}{\overline{F}}Q^{-1}\hat{F}\Big)\ . \tag{28}$$

Now we define Q^{-1} formally as

$$Q^{-1} = -\int_0^\infty ds \exp(sQ) , \tag{29}$$

where $\exp(sQ)$, representing the formal solution to the backward Kolmogorov equation $\partial_s u = Qu$, may be viewed as a stochastic shift operator. For example,

$$\exp(sQ)\hat{\rho}[\xi(0)] = E\{\hat{\rho}[\xi(s)]|\hat{\rho}[\xi(0)]\} , \tag{30}$$

where the right-hand-side stands for the expectation value of $\hat{\rho}$ at $z = s$, *given* the value of $\hat{\rho}$ at $z = 0$. Provided that the systems we are trying to model have finite correlation length, $\exp(sQ)\hat{F} = 0$ for $s \to \infty$. That is why the upper limit of the integration for Eq. (29) always gives zero. Now let us return to Eq. (28) and substitute Eq. (29) for Q^{-1}. The result is

$$\begin{aligned}
&\int d\xi \left[-\frac{\overline{P}}{2\pi v_0} \left(\frac{\partial}{\partial \phi} \overline{F}^{-1} \right) \hat{F} Q^{-1} \hat{F} \right] \\
&\quad + \int d\xi \left[-\frac{\overline{P}}{2\pi v_0} \overline{F}^{-1} \left(\frac{\partial}{\partial \phi} \hat{F} \right) Q^{-1} \hat{F} \right] \\
&= (2\pi v_0)^{-1} \left\{ \left(\frac{\partial}{\partial \phi} \overline{F}^{-1} \right) \int d\xi \, \overline{P} \int_0^\infty ds \langle \hat{F}(0) \hat{F}(s) \rangle \right. \\
&\quad \left. + \overline{F}^{-1} \int d\xi \, \overline{P} \int_0^\infty ds \left\langle \frac{\partial \hat{F}(0)}{\partial \phi} \hat{F}(s) \right\rangle \right\} \\
&= (2\pi v_0^2 \overline{F}^2)^{-1} \sin 2\phi [\rho_0 \alpha_{\rho\rho} \sin^2 \phi - K_0^{-1} \alpha_{KK} \cos^2 \phi \\
&\quad + (K_0^{-1} \cos^2 \phi - \rho_0 \sin^2 \phi) \alpha_{\rho K}] .
\end{aligned} \tag{31}$$

Here we have defined

$$\alpha_{\rho\rho} = \int_0^\infty ds\langle\rho(0)\rho(s)\rangle \ , \tag{32a}$$

$$\alpha_{KK} = \int_0^\infty ds\langle K^{-1}(0)K^{-1}(s)\rangle \ , \tag{32b}$$

$$\alpha_{\rho K} = \int_0^\infty ds\langle\hat{\rho}(0)\hat{K}^{-1}(s)\rangle = \alpha_{K\rho} \ . \tag{32c}$$

where $\langle\ \rangle$ denotes taking the expectation value with respect to $\boldsymbol{\xi}$. It is recognized that α's are the integrals of the autocorrelation and correlation functions for $\hat{\rho}$ and $\hat{K}^{-1}$. Combining Eqs. (31) and (27b) yields

$$g_1(\phi) = \frac{\beta}{\overline{F}} - \frac{\sin 2\phi[\rho_0\alpha_{\rho\rho}\sin^2\phi - K_0^{-1}\alpha_{KK}\cos^2\theta + (K_0^{-1}\cos^2\phi - \rho_0 sin^2\phi)\alpha_{\rho K}]}{2\pi v_0^2\overline{F}^3} \tag{33}$$

The knowledge of $g_1(\theta)$, plus the definition of Q^{-1} by Eq. (29), enable us to evaluate $\gamma = \gamma_1\omega^2$:

$$\gamma_1 = \frac{1}{2}\int_0^{2\pi} d\phi \int d\xi P^{(1)} \sin 2\phi[\rho - K^{-1}]$$

$$= \frac{1}{2}\left\{\int_0^{2\pi} d\phi \int d\xi \sin 2\phi[\rho - K^{-1}] \int_0^\infty ds\, \exp(sQ^*)(2\pi v_0)^{-1}\overline{P}\frac{\partial}{\partial\phi}\frac{\hat{F}}{\overline{F}}\right.$$

$$\left. + \int_0^{2\pi} d\phi \int d\xi\overline{P}(\xi_1,\xi_2)[\rho(\xi_1) - K^{-1}(\xi_2)]\sin 2\phi\, g_1(\phi)\right\} \ . \tag{34a}$$

It is noted that the term $\beta/\overline{F}$ in $g_1(\phi)$ integrates to zero for the same reason as $\gamma_0 = 0$ and therefore does not contribute. After carrying out the operations and simplifying the remaining, we get the final answer[12] as

$$\gamma = \gamma_1\omega^2 = \frac{1}{4}(\alpha_{\rho\rho} + \alpha_{KK} - 2\alpha_{\rho K})\frac{\omega^2}{v_0^2} \ . \tag{34b}$$

Equation (34b) tells us that to the leading order, the localization length diverges as ω^{-2} when $\omega \to 0$. Physically, this quadratic frequency dependence may be attributed to the ω^2 variation of the Rayleigh scattering in one dimension. The proportionality constant, $4v_0^2/(\alpha_{\rho\rho} + \alpha_{KK} -$

$2\alpha_{\rho K}$), on the other hand, does depend on both the mean property of the medium, $v_0 = (K_0/\rho_0)^{\frac{1}{2}}$, as well as the correlations of the fluctuating parts. For specific models, the α's may be evaluated explicitly. If we let $\hat{\rho} = 2\sigma_\rho \xi_1(z)$ and $\hat{K}^{-1} = 2\sigma_K \xi_2(z)$, then

$$\alpha_{\rho\rho} = \int_0^\infty ds\langle\rho(s)\rho(0)\rangle = 4\sigma_\rho^2 \int_0^\infty ds\langle\xi_1(s)\xi_1(0)\rangle \ . \tag{35a}$$

Now for model I where the layer thickness is constant $= \bar{a}$, we will make the assumption that since at low frequencies the wave cannot resolve the microstructures, the continuous Markovian model may still apply provided we allow the process $\boldsymbol{\xi}$ to start at random positions inside the first layer. The quantity $\langle\xi_1(s)\xi_1(0)\rangle$ can then be evaluated as follows. For $s > \bar{a}$, $\langle\xi_1(s)\xi_1(0)\rangle = 0$, and for $s < \bar{a}$

$$\langle\xi_1(s)\xi_1(0)\rangle = \left(1 - \frac{s}{\bar{a}}\right)\langle\xi_1^2\rangle = \frac{1}{12}\left(1 - \frac{s}{\bar{a}}\right) \ , \tag{35b}$$

where $\left(1 - \frac{s}{\bar{a}}\right)$ gives the probability that two points, separated by s, can still lie in the same layer. Substitution of Eq. (35b) into Eq. (35a) gives

$$\alpha_{\rho\rho} = \frac{1}{6}\sigma_\rho^2 \bar{a} \ . \tag{35c}$$

Similarly, $\alpha_{KK} = \sigma_K^2 \bar{a}/6$ and $\alpha_{\rho K} = 0$ because ξ_1 and ξ_2 are independent (although they jump simultaneously). That means

$$\gamma_1 = \frac{(\sigma_\rho^2 + \sigma_K^2)\bar{a}}{24v_0^2} \tag{36}$$

for model I. For model II, the only difference is that the layers have an exponential thickness distribution with mean $\bar{a}$. The continuous Markovian model is strictly applicable, and

$$\langle\xi_1(s)\xi_1(0)\rangle = \frac{1}{\bar{a}}\exp\left(-\frac{s}{\bar{a}}\right)\langle\xi_1^2\rangle = \frac{1}{12\bar{a}}\exp\left(-\frac{s}{\bar{a}}\right) \ . \tag{37}$$

Substitution of Eq. (37) into Eq. (35a) then yields $\alpha_{\rho\rho} = \sigma_\rho^2\bar{a}/3$. That means for model II, γ_1 is given by

$$\gamma_1 = \frac{(\sigma_\rho^2 + \sigma_K^2)\bar{a}}{12v_0^2} \ , \tag{38}$$

which differs from Eq. (36) by a factor of two. This prediction is indeed verified by numerical simulations as will be seen in Sec. 4.4.

For model III, the material parameters ρ and K^{-1} are obtained from model II by an exponential filter $E(z) = \exp(-z)(z \geq 0, E(z) = 0$ for $z < 0)$, i.e. $m(z) = E(z) \otimes \overline{m}(z)$, where $\overline{m}$ and m denote the material parameters for models II and III, respectively, and $\otimes$ means convolutions. Since the α's may be alternatively expressed as the power spectrum S_m of m at zero spatial frequency, i.e.

$$\int_0^\infty \langle m(s)m(0)\rangle ds = S_m(0) \,, \tag{39a}$$

it is clear that the low frequency localization length of model II and model III must be the same because

$$S_m(0) = S_{\overline{m}}(0) \cdot |J(0)|^2 = S_{\overline{m}}(0) \,, \tag{39b}$$

where $J(i\nu) = (1 + i\nu)^{-1}$ is the Fourier transform of $E(z)$, with ν denoting spatial frequency, and $|J(0)|^2$ is noted to be 1.

4.3. High Frequency Solution

In the limit of high frequencies, we expand $P(\phi, \xi_1 \xi_2)$ as

$$P = P^{(0)} + \frac{1}{\omega} P^{(1)} + \frac{1}{\omega^2} P^{(2)} + \ldots \tag{40}$$

Substitution of Eq. (40) into Eq. (9) gives

$$\gamma = c_0\omega + c_1 + \frac{c_2}{\omega} + \ldots \,, \tag{41a}$$

where

$$c_n = \frac{1}{2} \int_0^{2\pi} d\phi \int d\xi P^{(n)}(\phi, \xi) \sin 2\phi [\rho(\xi_1) - K^{-1}(\xi_2)] \,. \tag{41b}$$

The Fokker-Planck equation, Eq. (14), requires that

$$Q^* P^{(0)} + \frac{1}{\omega} Q^* P^{(1)} + \frac{1}{\omega^2} Q^* P^{(2)} + \ldots = -\omega \frac{\partial}{\partial \phi} F P^{(0)} - \frac{\partial}{\partial \phi} F P^{(1)} - \frac{1}{\omega} \frac{\partial}{\partial \phi} F P^{(2)} + \ldots \tag{42a}$$

By equating terms with the same powers of ω, we get

$$\frac{\partial}{\partial\phi} F P^{(0)} = 0 \,, \tag{42a}$$

and

$$Q^* P^{(n)} = -\frac{\partial}{\partial\phi} F P^{(n+1)} \,; n \geq 0 \,. \tag{42b}$$

Here $F = \rho \sin^2\phi + K^{-1}\cos^2\phi$ as dèfined before. Equation (42a) tells us that

$$P^{(0)} = g_0(\xi) F^{-1} \,, \tag{43}$$

where $g_0(\xi)$ is determined by the requirement that

$$\int_0^{2\pi} d\phi P(\phi, \xi) = \overline{P}(\xi) \,. \tag{44}$$

Since $P^{(0)}$ is the only term in P that is independent of ω, the normalization condition on P is equivalent to the normalization conditions on $P^{(0)}$. By substituting Eq. (43) into Eq. (44), we get $g_0(\xi) = (2\pi)^{-1}(\rho K^{-1})^{\frac{1}{2}} \overline{P}(\xi)$, or

$$P^{(0)} = \sqrt{\frac{\rho(\xi_1)}{K(\xi_2)}} \frac{\overline{P}(\xi_1, \xi_2)}{2\pi[\rho(\xi_1)\sin^2\phi + K^{-1}(\xi_2)\cos^2\phi]} \,. \tag{45}$$

It is now immediately obvious that $c_0 = 0$ because the ϕ integration of the product of $\sin 2\phi$, an odd function of ϕ, with F^{-1}, an even function of ϕ, is zero. This result is important because *it constitutes a proof that the localization length is non-decreasing as* $\omega \to \infty$. Since $\gamma = c_1 + c_2/\omega + \ldots$, the localization length can either saturate to a constant value ($c_1 \neq 0$), or increase with frequency ($c_1 = 0$). To calculate c_1, we use $P^{(0)}$ as the input to the next-order equation

$$\frac{\partial}{\partial\phi} F P^{(1)} = Q^* P^{(0)} \,, \tag{46a}$$

or

$$P^{(1)} = -\frac{1}{2\pi F} Q^* \sqrt{\frac{\rho(\xi_1)}{K(\xi_2)}} \overline{P}(\xi_1, \xi_2) \times \int_0^{\phi} \frac{d\phi'}{[\rho(\xi_1)\sin^2\phi' + K^{-1}(\xi_2)\cos^2\phi']} + g_1(\xi) F^{-1} \,. \tag{46b}$$

Here $g_1(\boldsymbol{\xi})$ can be obtained by the condition that

$$\int_0^{2\pi} d\phi P^{(1)}(\phi, \xi_1, \xi_2) = 0 \ . \tag{46c}$$

However, there is no need to determine $g_1(\boldsymbol{\xi})$ because for the calculation of γ the term $g_1(\boldsymbol{\xi})/F$ will integrate to zero for the same reason that $c_0 = 0$. Now the constant c_1 may be expressed as[6]

$$c_1 = -\frac{1}{4\pi} \int d\boldsymbol{\xi} \int_0^{2\pi} d\phi \frac{\sin 2\phi [\rho(\xi_1) - K^{-1}(\xi_2)]}{[\rho(\xi_1)\sin^2\phi + K^{-1}(\xi_2)\cos^2\phi]}$$

$$\cdot \left\{ Q^* \overline{P}(\xi_1, \xi_2) \sqrt{\frac{\rho(\xi_1)}{K(\xi_2)}} \int_0^{\phi} \frac{d\phi'}{[\rho(\xi_1)\sin^2\phi' + K^{-1}(\xi_2)\cos^2\phi']} \right\}$$

$$= -\frac{1}{4\pi} \int d\boldsymbol{\xi}\, \overline{P}(\xi_1, \xi_2) \sqrt{\frac{\rho(\xi_1)}{K(\xi_2)}} \int_0^{2\pi} d\phi \sin 2\phi$$

$$\times \int_0^{\phi} \frac{d\phi'}{\rho \sin^2\phi' + K^{-1}\cos^2\phi'} Q\left[\frac{\rho(\xi_1) - K^{-1}(\xi_2)}{\rho(\xi_1)\sin^2\phi + K^{-1}(\xi_2)\cos^2\phi}\right] , \tag{47}$$

where we have used the adjoint property of the operator Q^*. By carrying out the ϕ' integration explicitly, we get

$$c_1 = -\frac{1}{4\pi} \int d\boldsymbol{\xi}\, \overline{P}(\xi_1, \xi_2)$$
$$\times \int_0^{2\pi} d\phi \arctan\left(\sqrt{\rho(\xi_1)K(\xi_2)}\tan\phi\right) \sin 2\phi$$
$$\cdot Q\left[\frac{\rho(\xi_1) - K^{-1}(\xi_2)}{\rho(\xi_1)\sin^2\phi + K^{-1}(\xi_2)\cos^2\phi}\right] , \tag{48}$$

where the arctan function is understood to be the branch which is zero when $\phi = 0$, and is monotonically increasing. In contrast to the

low-frequency case, here we cannot go any further without explicitly evaluating the Q operation. This is physically reasonable because at high frequencies the wave would be able to resolve the inhomogeneities of the medium, and the value of c_1 is therefore dependent on the local details of the model as expressed by the operator Q. That means there should be significant difference between the three models. However, for models I and II if one makes the assumption that at high frequencies the scatterings at interfaces occur incoherently, then the two models should be indistinguishable in that limit.

To evaluate c_1, we note that the integration implicit in the operator Q can be performed analytically. The actual numerical calculation therefore involves only a double integral. For model III, however, the Q operator is defined by Eq. (12b), with ρ and K^{-1} the functionals of η_1 and η_2, respectively. Therefore,

$$c_1 = -\frac{1}{4\pi}\int d\boldsymbol{\xi} d\boldsymbol{\eta}\, \overline{P}(\boldsymbol{\xi},\boldsymbol{\eta}) \int_0^{2\pi} d\phi \arctan\left(\sqrt{\rho(\eta_1)K(\eta_2)}\tan\phi\right)\sin 2\phi \times Q\left[\frac{\rho K - 1}{\rho K \sin^2\phi + \cos^2\phi}\right], \tag{49a}$$

where

$$Q = Q_{\boldsymbol{\epsilon}} + (\xi_1 - \eta_1)\frac{\partial}{\partial \eta_1} + (\xi_2 - \eta_2)\frac{\partial}{\partial \eta_2} = Q_{\boldsymbol{\epsilon}} + f\frac{\partial}{\partial \rho} + g\frac{\partial}{\partial K^{-1}}, \tag{49b}$$

with $f = d\rho/dz = \rho_{\mathrm{II}} - \rho_{\mathrm{III}}$ and $g = dK^{-1}/dz = K_{\mathrm{II}}^{-1} - K_{\mathrm{III}}^{-1}$, and $\overline{P}$ is the joint stationary distributions for $\boldsymbol{\xi}$ and $\boldsymbol{\eta}$. From Eq. (49a) it is easy to see that the effect of $Q_{\boldsymbol{\epsilon}}$ is to give zero since the operand is independent of $\boldsymbol{\xi}$. The remaining derivative operations may be carried out explicitly to obtain

$$c_1 = -\frac{1}{4\pi}E\left[\int_0^{2\pi} d\phi \arctan\left(\sqrt{\rho K}\tan\phi\right) \times \frac{\sin 2\phi}{\rho K \sin^2\phi + \cos^2\phi}\rho K(f\rho^{-1} - gK)\right]. \tag{50a}$$

Here $E[\ ]$ denotes the operation of taking the expectations value with respect to the variables η and ξ. We note, however, that $f\rho^{-1} = (d\rho/dz)\rho^{-1} = d\ln\rho/dz$ and $gK = -d\ln K/dz$. Therefore $\rho K(f\rho^{-1} - gK)$ may be expressed as $\rho K\, d\ln(\rho K)/dz = d(\rho K)/dz$. Equation (50a) may be rewritten as

$$c_1 = -\frac{1}{4\pi}E\left[\frac{d}{dz}\int_0^{\rho K}\int_0^{2\pi}\arctan(\sqrt{u}\tan\phi)\frac{\sin\phi}{u\sin^2\phi+\cos^2\phi}d\phi\,du\right]. \tag{50b}$$

By interchanging the order of the d/dz operation and the $E[\ ]$ operation, we get $c_1 = 0$ because the stationary expectation value is independent of z by definition.

The fact that $c_1 = 0$ for continuous random models means that $l(\omega)$ diverges as $\omega \to \infty$. This difference in the qualitative behaviors between models I, II and III may be understood physically as follows. For the discontinuous models, the reflection and transmission coefficients at a sharp interface are frequency independent. When the phase coherence between the different scattering events is lost at high frequencies, the localization length must also be frequency independent as shown. However, when the interface is fuzzy and continuous, the reflection coefficient at each interface is expected to decrease as the wavelength becomes smaller than the size of the interface region. This is because the wave would begin to perceive the environment as slowly varying and the wave transmission is consequently increased.

4.4. Oblique Incidence

At non-normal incidence, it becomes important to distinguish between the electromagnetic wave and the elastic wave, and the behavior of differing polarizations could be dramatic.[9] In this section we will consider only the electromagnetic case, since the elastic case would require significant modification of the formalism derived so far.

If we let H denote the y-component of the magnetic field, E the x-component of the electric field, θ the incident angle with respect to te normal (z-axis) and ε_0, μ_0 the mean value of the dielectric constant and the magnetic permeability, respectively, then the wave equation may be

written as

$$\frac{d}{dz}\begin{pmatrix} H \\ E \end{pmatrix} = \frac{\omega}{c}\begin{bmatrix} 0 & \varepsilon(z) \\ -\mu(z) + \dfrac{\mu_0 \varepsilon_0 \sin^2\theta}{\varepsilon(z)} & 0 \end{bmatrix}\begin{pmatrix} H \\ E \end{pmatrix} \tag{51a}$$

for the polarization where the xz plane is the plane of incidence so that the H vector is perpendicular to it. We will denote this configuration the H-polarization. Analogously, we define the E-polarization as that configuration when the yz plane is the plane of incidence. In that case the wave equation is given by

$$\frac{d}{dz}\begin{pmatrix} H \\ E \end{pmatrix} = \frac{\omega}{c}\begin{bmatrix} 0 & \varepsilon(z) - \dfrac{\mu_0 \sin^2\theta}{\mu(z)} \\ -\mu(z) & 0 \end{bmatrix}\begin{pmatrix} H \\ E \end{pmatrix} . \tag{51b}$$

In the above we have assumed that the wave is incident from a homogeneous halfspace with material parameters ε_0 and μ_0. Comparison of Eq. (51) and Eq. (5) shows that if we make the identification

$$\rho(z) \to \frac{\varepsilon(z)}{c} , \tag{51c}$$

$$K^{-1}(z) \to \frac{\mu(z)}{c} - \frac{\mu_0 \varepsilon_0 \sin^2\theta}{c\varepsilon(z)} , \tag{51d}$$

for the H-polarization and

$$\rho(z) \to \frac{\varepsilon(z)}{c} - \frac{\mu_0 \varepsilon_0 \sin^2\theta}{c\mu(z)} , \tag{51e}$$

$$K^{-1}(z) \to \frac{\mu(z)}{c} , \tag{51f}$$

for the E-polarization, then the low- and the high-frequency localization length solutions developed in the previous sections may be carried through with minimal changes. However, the important point to note here is that the fluctuating part of $\rho(= \rho_0(1+\hat{\rho}))$, $\hat{\rho}$, and the fluctuating part of $K^{-1}(= K_0^{-1}(1+\hat{K}^{-1}))$, $\hat{K}^{-1}$, are no longer independent as

before but are correlated. For example, in the case of H-polarization if we write $\varepsilon = \varepsilon_0(1+\hat{\varepsilon})$, $\varepsilon^{-1} = \bar{\varepsilon}_{\rm inv}(1+\hat{\varepsilon}_{\rm inv})$, and $\mu = \mu_0(1+\hat{\mu})$, then

$$\hat{\rho} = \hat{\varepsilon} \ , \tag{52a}$$

$$\hat{K}^{-1} = \frac{\hat{\mu} - \varepsilon_0 \bar{\varepsilon}_{\rm inv} \sin^2\theta \ \hat{\varepsilon}_{\rm inv}}{1 - \varepsilon_0 \bar{\varepsilon}_{\rm inv} \sin^2\theta} \ . \tag{52b}$$

Since $\varepsilon_0^{-1} \neq \bar{\varepsilon}_{\rm inv}$ in general, $\hat{\varepsilon}$ and $\hat{\varepsilon}_{\rm inv}$ cannot be independent, and we have a case of built-in correlation between $\hat{\rho}$ and $\hat{K}^{-1}$. By expressing

$$\hat{\varepsilon} = 2\sigma_\varepsilon \xi_1 \ , \tag{53a}$$

$$\hat{\mu} = 2\sigma_\mu \xi_2 \ , \tag{53b}$$

we get

$$\bar{\varepsilon}_{\rm inv} = \int_{-\frac{1}{2}}^{\frac{1}{2}} \frac{d\xi_1}{\varepsilon_0(1+2\sigma_\varepsilon\xi_1)} = \frac{1}{2\sigma_\varepsilon\varepsilon_0} \ln\left(\frac{1+\sigma_\varepsilon}{1-\sigma_\varepsilon}\right) \ , \tag{53c}$$

and

$$\hat{\varepsilon}_{\rm inv} = \frac{2\sigma_\varepsilon}{(1+2\sigma_\varepsilon\xi_1)} \left[\ln\left(\frac{1+\sigma_\varepsilon}{1-\sigma_\varepsilon}\right)\right]^{-1} - 1 \ . \tag{53d}$$

For the low frequency limit, the calculation of $\alpha_{\rho\rho}$, α_{KK}, and $\alpha_{\rho K}$ for model I leads to

$$\gamma^{(H)} \simeq \gamma_1^{(H)}\omega^2 = \frac{1}{24}\left[\sigma_\varepsilon^2 + \frac{\sigma_\mu^2 + M\sin^4\theta}{(1-C\sin^2\theta)^2} + \frac{N\sin^2\theta}{1-C\sin^2\theta}\right] \times (1-C\sin^2\theta)\frac{\varepsilon_0\mu_0}{c^2}\omega^2 \ , \tag{54a}$$

where the constants C, M, N are defined by

$$C = \frac{1}{2\sigma_\varepsilon} \ln\left(\frac{1+\sigma_\varepsilon}{1-\sigma_\varepsilon}\right) \ , \tag{54b}$$

$$M = 3\left[\frac{1}{1-\sigma_\varepsilon^2} - C^2\right] \ , \tag{54c}$$

$$N = 6(1-C) \ . \tag{54d}$$

Results for models II and III can be obtained from Eq. (54a) by multiplying $\gamma_1^{(H)}$ by a factor of 2. It is seen that at $\theta = 0$, Eq. (54a) recovers the known result, Eq. (36), and for non-magnetic material ($\sigma_\mu = 0$) and $\sigma_\epsilon \ll 1$, Eq. (54a) simplifies as

$$\gamma^{(H)} \simeq \gamma_1^{(H)}\omega^2 = \frac{\sigma_\epsilon^2}{24}(1 - \tan^2\theta)\cos^2\theta\frac{\epsilon_0\mu_0}{c^2}\omega^2 \tag{55}$$

to order σ_ϵ^2. We note that at $\theta = 45°$, $\gamma_1^{(H)} = 0$ so that the localization length actually diverges faster than ω^2. This phenomenon has its origin in the well-known Brewster effect[9,17] for reflection from a plane interface. Namely, when $\sigma_\epsilon \ll 1$ the incident wave at 45° is roughly perpendicular to the reflected wave as shown in Fig. 3. That means the E-vector of the incident wave is parallel to the direction of the reflected wave. If one regards the reflected wave as generated by dipoles excited by the incident E-field, then there can be no wave amplitude in the reflection direction due to the fact that dipoles do not radiate in the direction of its oscillation. When σ_ϵ is not small, Eq. (54a) generally has a zero at some value of $\theta_B \neq 45°$. The actual value of the localization length usually does not diverge at such angle, since true divergence would require $\gamma_n^{(H)} = 0$ to all orders of n. However, the value of the localization length can be expected to be orders of magnitude larger at θ_B than that at normal incidence. This effect is denoted as the Brewster anomaly in accordance with its physical origin. An exception to the above description is that of the binary random medium, where true divergence of l can be achieved at certain incident angle. This is due to the fact that if θ_B is the Brewster angle for a wave going from medium 1 to medium 2, then the refracted angle in medium 2 is also exactly the Brewster angle in going from medium 2 to medium 1. Therefore this is a case where the deterministic Brewster effect completely overcomes the stochastic effect of localization.

For the E-polarization, $\gamma_1^{(E)}$ has exactly the same form as that of $\gamma_1^{(H)}$, Eq. (54a), except the roles of σ_ϵ and σ_μ are now interchanged. Therefore, $\gamma_1^{(E)}$ would have the same Brewster anomaly for a random magnetic material. However, if $\sigma_\mu = 0$, then

$$\gamma \simeq \gamma_1^{(E)}\omega^2 = \frac{\sigma_\epsilon^2}{24}\sec^2\theta\frac{\omega^2}{v_0^2}\ , \tag{56}$$

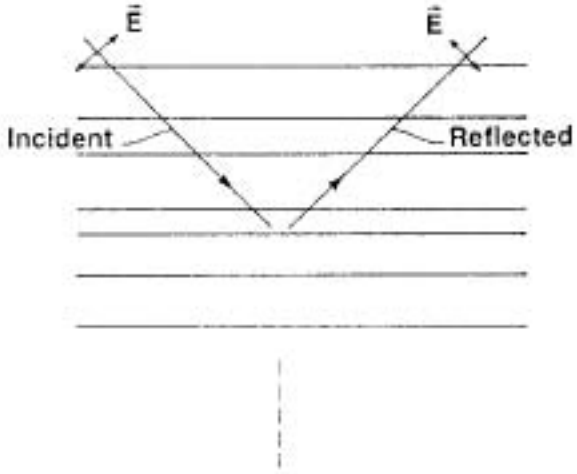

Fig. 3. Schematic diagram illustrating the H-polarized incident and scattered beams in a randomly-layered medium with small material fluctuations. Brewster effect occurs when the incident **E** field is parallel to the scattering direction.

for model I, and $\gamma_1^{(E)}$ is a factor of 2 larger for models II and III. It is seen that the angular dependence of $\gamma_1^{(E)}$ is perfectly regular. At high frequencies, the same formalism as before carries through with the different definitions now for ρ and K^{-1}. Since one cannot get explicit formulas for c_1 anyway, the correspondence with ρ and K^{-1} is as far as one can go without getting into actual numerical computations.

4.5. Numerical Simulations

To summarize the results of the previous sections, we see that to the leading order, the frequency dependence of the localization length may be expressed as $l \sim \omega^{-2}$ for $\omega \to 0$ and $l \sim$ constant or increases as a power of ω for $\omega \to \infty$, where the proportionality constants are calculable from material parameters and model statistics. There is also strong polarization dependence at oblique incidence. To verify this form for $l(\omega)$ and to actually see the behavior at intermediate frequencies where the wavelength is comparable to the correlation length of the inhomogeneities, we use the transfer-matrix algorithm for numerically calculating the transmission coefficient T through a finite segment L of the random medium. Since $T \sim \exp(-\gamma L)$, the localization length is obtained as $l = -\langle \ln|T|/L\rangle^{-1}$, where $\langle\ \rangle$ now denotes configurational averaging. From the ergodic theorem, we expect this to be the same as

taking the expectations value with respect to ξ.

The transfer-matrix algorithm is based on the assumption that the layered medium is composed of homogeneous layers within each of which the general solution to the wave equation may be expressed as

$$p_n(z) = A_n \exp\left[ik_n\left(z - z_n + \frac{a_n}{2}\right)\right] + B_n \exp\left[-ik_n\left(z - z_n + \frac{a_n}{2}\right)\right], \tag{57}$$

where p_n denotes pressure in the nth layer, a_n denotes the layer thickness, z_n is the coordinate of the interface between the nth and the $(n+1)$th layers, $k_n = \omega/(K_n/\rho_n)^{\frac{1}{2}}$, and A_n and B_n are the coefficients for the forward-traveling and the backward-traveling waves in the nth layer, respectively. If the material parameters ρ and K^{-1} are continuously-varying, such as in model III, the medium may be approximated by fine, piecewise-constant layerings so that Eq. (57) is approximately valid in each layer. To relate the solution in the nth layer to that of the $(n+1)$th layer requires that the boundary conditions, $p_n(z_n) = p_{n+1}(z_n)$ and $u_n(z_n) = i(\omega\rho_n)^{-1}\partial p_n/\partial z = i(\omega\rho_{n+1})^{-1}\partial p_{n+1}/\partial z = u_{n+1}(z_n)$, be satisfied at the interface $z = z_n$. The net result is that the coefficients A_n, B_n are related to coefficients A_{n+1}, B_{n+1} through the following matrix equation:

$$\begin{pmatrix} A_{n+1} \\ B_{n+1} \end{pmatrix} = t_n \begin{pmatrix} A_n \\ B_n \end{pmatrix}, \tag{58a}$$

$$t_n = \frac{1}{2}\begin{bmatrix} \left(1 + \frac{I_{n+1}}{I_n}\right)\exp\left[i(\nu_n + \nu_{n+1})\right] & \left(1 - \frac{I_{n+1}}{I_n}\right)\exp\left[-i(\nu_n - \nu_{n+1})\right] \\ \left(1 - \frac{I_{n+1}}{I_n}\right)\exp\left[i(\nu_n - \nu_{n+1})\right] & \left(1 + \frac{I_{n+1}}{I_n}\right)\exp\left[-i(\nu_n + \nu_{n+1})\right] \end{bmatrix}, \tag{58b}$$

where $I_n = \sqrt{\rho_n K_n}$ and $\nu_n = k_n a_n/2$. If there are a total of N layers in distance L, then

$$\begin{pmatrix} T \\ 0 \end{pmatrix} = t \begin{pmatrix} 1 \\ R \end{pmatrix}. \tag{59a}$$

$$t = t_N t_{N-1} \ldots t_1 t_0 . \tag{59b}$$

Here R is the reflection coefficient and T the transmission coefficient. By labeling the elements of the t matrix as

$$t = \begin{pmatrix} t_{11} & t_{12} \\ t_{12}^* & t_{11}^* \end{pmatrix},$$

we get

$$T = (|t_{11}|^2 - |t_{12}|^2)/t_{11}^* \ . \tag{60}$$

By averaging $-\ln|T|/L$ over many configurations, a numerical value of the localization length is then obtained as $-\langle \ln|T|/L\rangle^{-1}$.

In Fig. 4 the computed $l(\omega)$ is plotted versus the wavelength $\lambda = 2\pi\sqrt{K_0/\rho_0}/\omega$ for model I (equal layer thickness) at two distinct values of $\sigma = \sigma_\rho = \sigma_K = 0.3, 0.8$. Each data point represents the result of averaging over 40 configurations. The dashed lines denote the low-frequency and the high-frequency limiting behaviors evaluated from the analytical formulas presented in the last sections. Good agreement is clearly seen. In the intermediate frequency regime, the numerical simulation results exhibit pronounced oscillations. They are interpretable as a remnant of a periodic system where there are bands of delocalized states. In this regard, we wish to note that if instead of a continuous distribution for ρ and K^{-1} we have a binary system (i.e. $\rho = \rho_1, \rho_2, K = K_1, K_2$), then the system may not be regarded as random (in the sense of having a finite localization length at all finite frequencies) unless the layer thickness of *both* components are allowed to vary randomly. This is due to the fact that if one component has a fixed thickness, then total transmission through that component can be achieved whenever the 1/4-wavelength condition is satisfied (in exact analogy with the anti-reflection coating condition). The wave would then be traveling in an equivalent one-component medium and the localization length diverges at these specific frequencies.

In Fig. 5 the computed $l(\omega)$ for model II is plotted as a function of λ for three values of $\sigma = \sigma_\rho = \rho_K = 0.1, 0.3, 0.9$. Each data point is the result of averaging over 40 configurations. The dashed lines again represent the predicted asymptotic behaviors. They are seen to agree very well with the simulated values in the high- and low-frequency limits. In particular, we note that the prediction of a factor of 2 difference in the low frequency values of $l(\omega)$ for models I and II is indeed verified (comparing the case for $\sigma = 0.3$). Except for statistical fluctuations, the behavior of $l(\omega)$ in this case is essentially a smooth interpolation between the two limits. In fact, the form $c_1^{-1} + 6v_0^2/(\sigma^2\omega^2\bar{a})$ is an accurate representation for $l(\omega)$ over the entire frequency range.

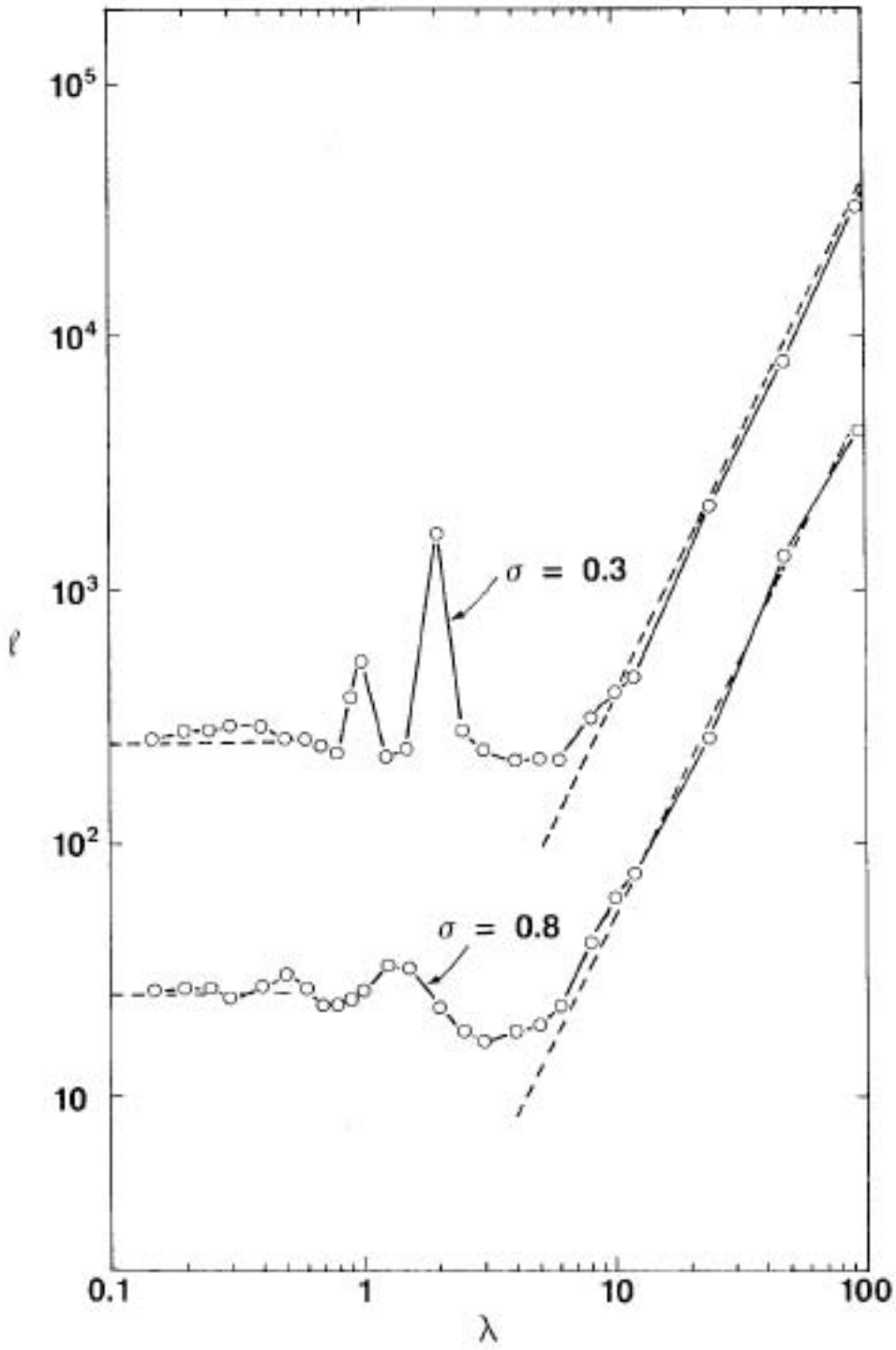

Fig. 4. Localization length plotted as a function of wavelength for model I, calculated at two values of the fluctuation parameter $\sigma = \sigma_\rho = \sigma_K = 0.3$, 0.8 and $\rho_0 = K_0 = 1$. Both l and λ are in units of the layer thickness $\bar{a}$. Dashed lines denote the predictions of the analytic theory in the high- and low-frequency limits. Each data point is an average of 40 configurations.

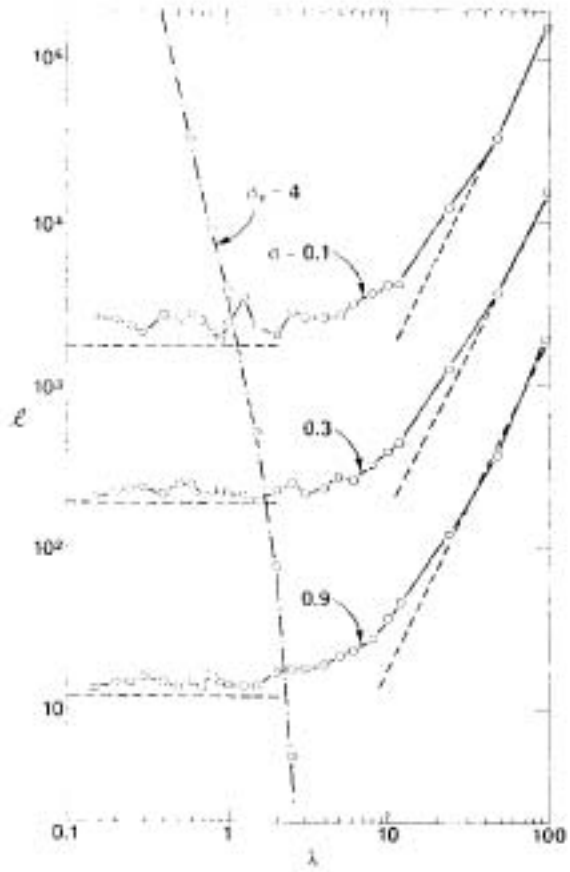

Fig. 5. Localization length plotted as a function of wavelength for model II, calculated at three different values of the parameter $\sigma = \sigma_\rho = \sigma_K = 0.1$, 0.3, 0.9 and $\rho_0 = K_0 = 1$. Both l and λ are in units of the average layer thickness $\bar{a}$. Dashed lines denote the predictions of the analytic theory in the high- and low-frequency limits. Each data point represents an average of 40 configurations. Comparison with Fig. 4 for the case of $\sigma = 0.3$ clearly shows a factor of 2 in the low-frequency value of l. The dashed-dot line denote the localization length for a quantum particle described by the Schrödinger equation.

Also shown in Fig. 5 by a dot-dashed line is the localization length behavior for a quantum particle whose behavior is governed by the Schrödinger equation with a random potential V. In this case we define $\lambda = 2\pi\hbar/\sqrt{2mE}$, where $\hbar$ is Planck's constant, m the mass of the particle and E its energy defined relative to the lower bound of V. The localization length, again calculated by the transfer-matrix method, clearly shows a frequency dependence that is opposite to the classical wave behavior. This is due to the fact that whereas the reflection coefficient at

a sharp interface is independent of the frequency for the classical waves, the quantum particle always becomes more transmitting as its energy increases. Also, the classical wave scattering tends to become weaker as energy decreases whereas the quantum particle scattering tends to become stronger because the particle no longer has enough energy to overcome the potential barrier. As a result, there is no minimum value for the localization length of a quantum particle in random potentials.

For model III, where the material parameters vary continuously, the frequency dependence of the localization length is plotted in Fig. 6 for three cases where the material parameters are obtained from those of Fig. 5 through a convolution with an exponential filter. It is seen that $l(\omega)$ has a well-defined minimum value at $\lambda \sim 10\bar{a}$. The fact that $l(\omega)$ diverges at high frequencies is indeed verified, and the low-frequency behavior agrees with that of model II as expected. From our data the divergence at high frequencies seems to follow the form $l \sim \omega^2$.

Common to the localization length of all the three models is the fact that there is a well-defined minimum value. Furthermore, this minimum localization length is generally orders of magnitude larger than $\bar{a}$. Comparisons with the Schrödinger wave localization behavior indicates that there is no counterpart to the minimum localization length in the quantum case.

For oblique incidence of electromagnetic waves, we have evaluated the E- and H-polarized localization lengths (along the z direction) in a model II-type medium. In Fig. 7, values of l for the two polarizations are plotted as a function of angle of incidence at $\lambda/\bar{a} = 48$. In the present case we have assumed that $\sigma_\epsilon = 0.3$ and $\sigma_\mu = 0$, and the transfer matrix for the H-polarization has exactly the same form as Eq. (58b) except now $I_n = \varepsilon_n/\sqrt{(\varepsilon_n/\varepsilon_0) - \sin^2\theta}$ and $\nu_n = \omega a_n \sqrt{\varepsilon_n - \varepsilon_0 \sin^2\theta}/2c$, where θ is the angle of incidence at the interface between the homogeneous medium (dielectric constant ε_0) and the random medium (dielectric constant $\varepsilon_0[1 + 2\sigma_\epsilon \xi(z)]$). For the E-polarization the only difference in the transfer matrix is that $I_n = 1/\sqrt{(\varepsilon_n/\varepsilon_0) - \sin^2\theta}$. The agreement between theory and data is seen to be excellent for all angles up to the critical angle of total internal reflection (calculated in the effective-medium sense). The analytical formulas are then expected to

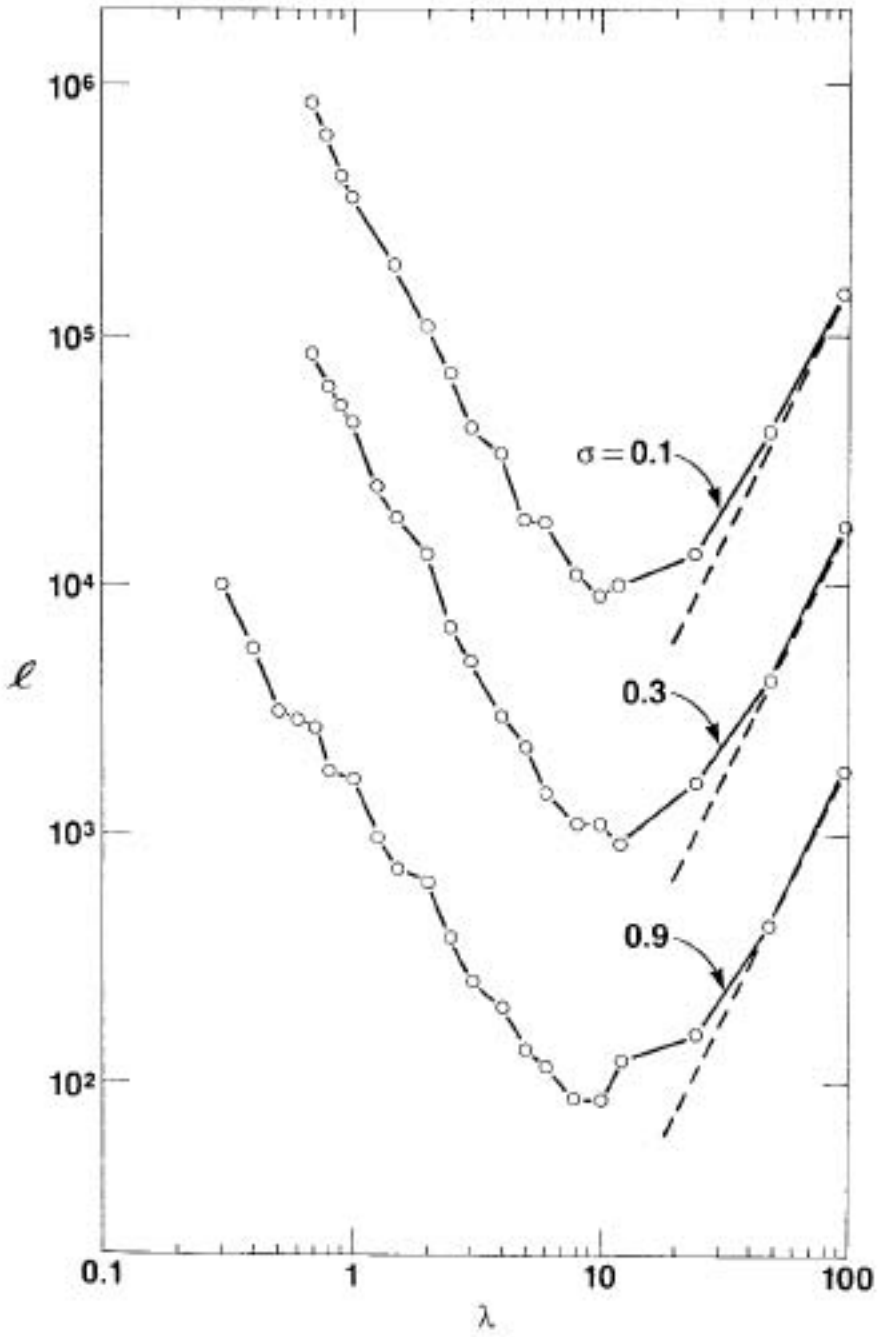

Fig. 6. Localization length plotted as a function of wavelength for model III, calculated for the materials obtained from Fig. 5 through the convolution with an exponential filter. Both l and λ are in units of $\bar{a}$ defined by model II. Dashed lines denotes the prediction of the low frequency theory. Each data point is an average of 40 configurations.

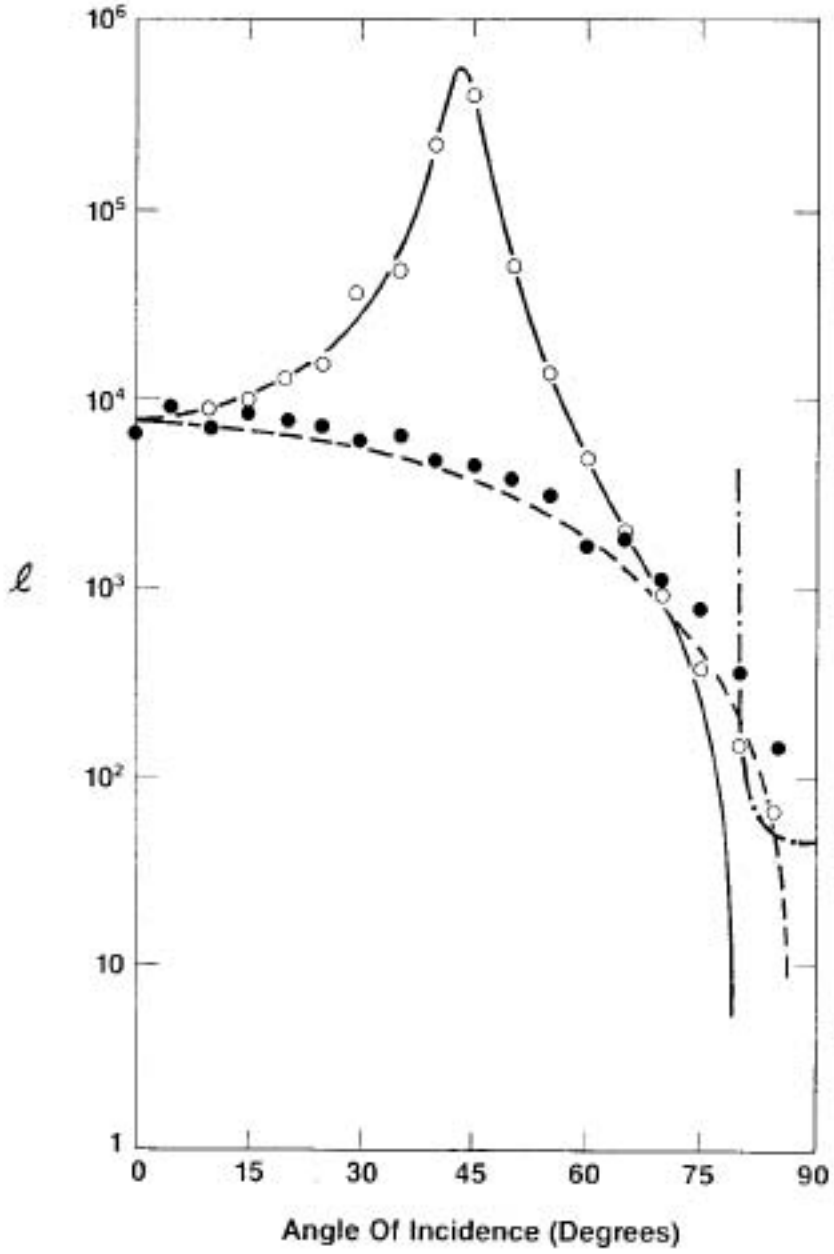

Fig. 7. Localization length in units of mean layer thickness $\bar{a}$ plotted as a function of incidence angle for $\lambda = 48\bar{a}$. The dielectric constant $\varepsilon(z)$ of the random medium is defined in the text. Open circles are results of Monte Carlo simulation for H-polarized light, and solid circles are for E-polarized light. Solid and dashed lines are calculated from the long-wavelength theory for the H- and the E-polarized waves, respectively. The dash-dot curve indicates the evanescent decay length beyond the critical angle of the H-polarized light calculated in the effective-medium theory.

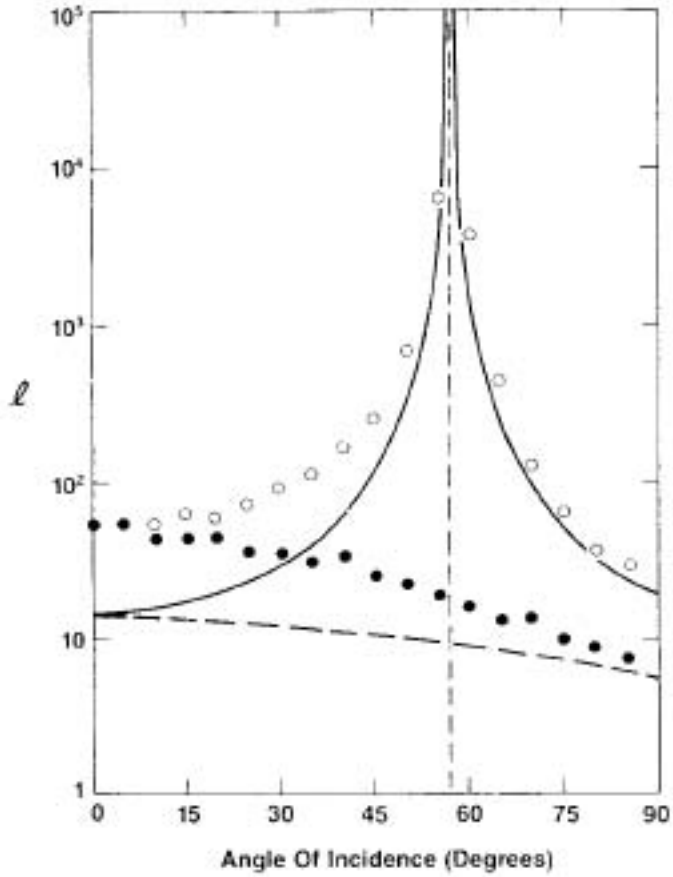

Fig. 8. Localization length in units of mean layer thickness $\bar{a}$ plotted as a function of incidence angle for $\lambda = 5\bar{a}$. The random medium is a binary layered system with $\varepsilon_a = \varepsilon_0$ and $\varepsilon_b = 2.42\varepsilon_0$. Open circles are results of simulation for H-polarized light, and solid circles are for E-polarized light. Solid and dashed curves are calculated from the long-wavelength theory for the H- and E-polarized waves, respectively.

fail due to the divergence of the fluctuations in the material parameters (e.g. see Eq. (52b)). However, an effective medium estimate of the evanescent decay length beyond the critical angle for the H-polarization yields reasonable agreement with the data. From the figure it is clear that the Brewster anomaly enhances the localization length of the H-polarized wave by two orders of magnitude with a fairly wide angular spread. The maximum occurs at $\theta \simeq 45°$ as predicted.

In Fig. 8 we show a case for binary layered system with $\varepsilon_a = \varepsilon_0$, $\varepsilon_b = 2.42\varepsilon_0$ and $\lambda = 5\bar{a}$. Since the wavelength is now comparable to $\bar{a}$, the low frequency theory is no longer expected to be quantitatively correct. Nevertheless, the divergence of the H-polarization localization

length and the position of where it occurs for the binary system,

$$\theta_B = \sin^{-1} \sqrt{\frac{\varepsilon_a \varepsilon_b}{\varepsilon_0(\varepsilon_a + \varepsilon_b)}} , \tag{61}$$

are still predicted accurately.

5. LOCALIZATION CHARACTERISTICS IN THE TIME DOMAIN

5.1. Formulation

We would now like to consider the response of a randomly-layered halfspace to a transient pressure pulse.[3-5] Since the problem is linear, for the case of the matched-medium boundary condition the interface pressure variation as a function of time τ can be written formally as

$$p(\tau) = (2\pi)^{-1} \int_{-\infty}^{\infty} d\omega \exp(i\omega\tau) f(\omega) R(\omega) , \tag{62}$$

where $f(\omega)$ is the pulse frequency spectrum and $R(\omega)$ the reflection coefficient. Based on the consideration of pulse multiple scattering, the function $p(\tau)$ is expected to have a fluctuating character. Therefore what we would like to study is the power spectrum of the response, $S(\tau, \omega)$. From the definition of the power spectrum we have

$$\begin{aligned} \langle p(\tau) p(\tau + t) \rangle &= (2\pi)^{-2} \int_{-\infty}^{\infty} d\omega_1 \int_{-\infty}^{\infty} d\omega_2 f(\omega_1) f^*(\omega_2) \\ &\quad \times \exp(-i\omega_2 t) \langle R(\omega_1) R^*(\omega_2) \rangle \exp[i(\omega_1 - \omega_2)\tau] \\ &= (2\pi)^{-1} \int_{-\infty}^{\infty} d\omega \exp(-i\omega t) S\left(\tau + \frac{t}{2}, \omega\right) , \end{aligned} \tag{63a}$$

where

$$\begin{aligned} S(\tau, \omega) &= (2\pi)^{-1} \int_{-\infty}^{\infty} d\Delta_\omega f\left(\omega - \frac{\Delta_\omega}{2}\right) f^*\left(\omega + \frac{\Delta_\omega}{2}\right) \\ &\quad \times \exp(-i\Delta_\omega \tau) U_1(\Delta_\omega, \omega) , \end{aligned} \tag{63b}$$

$$U_1(\Delta_\omega,\omega) = \langle R\Big(\omega - \frac{\Delta_\omega}{2}\Big) R^*\Big(\omega + \frac{\Delta_\omega}{2}\Big)\rangle \ . \tag{63c}$$

Here $\omega = (\omega_1 + \omega_2)/2$, $\Delta_\omega = \omega_2 - \omega_1$ denotes the frequency difference, and the subscript 1 denotes the case of the matched-medium interface boundary condition. From Eq. (63c) it is clear that $U_1(0,\omega) = 1$. One also intuitively expects $U_1(\infty,\omega) = 0$. If one assumes that $U_1(\Delta_\omega,\omega) \sim \delta(\Delta_\omega)$, i.e. $R(\omega_1)$ and $R(\omega_2)$ are not correlated unless $\omega_1 = \omega_2$, then

$$S(\tau,\omega) \propto |f(\omega)|^2$$

becomes independent of τ as one would expect for stationary noise. However, in reality we expect $R(\omega_1)$ and $R(\omega_2)$ to be correlated over a frequency range $\Delta\omega$ that is small compared to ω. In that case S may be written as

$$S(\tau,\omega) \cong |f(\omega)|^2 \cdot N(\tau,\omega) \ , \tag{64a}$$

$$N(\tau,\omega) = (2\pi)^{-1} \int_{-\infty}^{\infty} d\Delta_\omega \exp(-i\Delta_\omega \tau) U_1(\Delta_\omega,\omega) \ , \tag{64b}$$

where $N(\tau,\omega)$ denotes the noise spectrum and is seen to be just the Fourier transform of the correlation function for the reflection coefficient at two different frequencies. Since Δ_ω and τ are conjugate variables as evidenced in Eq. (64b), a finite correlation range $\Delta\omega$ for the function $U_1(\Delta_\omega,\omega)$ would imply a definite time scale $(\Delta\omega)^{-1}$ for the non-stationarity of the noise spectrum $N(\tau,\omega)$. What we are going to show, both analytically and numerically, is that U_1 is a smoothly decaying function governed by only one width parameter $\Delta\omega$. Moreover, $\Delta\omega \sim l^{-1}(\omega)$ so that the time scale of non-stationarity in the multiple scattering noise is determined by none other than the localization length.[4]

From Eq. (64) it is clear that in order to make mathematical progress we must evaluate the function $U_1(\Delta_\omega,\omega)$ as defined by Eq. (63c). To this end let us first non-dimensionalize and transform the wave equation for p and w, Eq. (2), into a form for the forward-

and backward-traveling wave amplitudes A and B:

$$\frac{d}{dz}\begin{bmatrix} A \\ B \end{bmatrix} = i\omega \begin{bmatrix} g & -h\exp(2i\omega z) \\ h\exp(2i\omega z) & -g \end{bmatrix} \begin{bmatrix} A \\ B \end{bmatrix} , \tag{65a}$$

where we have assumed harmonic time dependence for p and w, $g = (\hat{\rho} + \hat{K}^{-1})/2$, $h = (\hat{\rho} - \hat{K}^{-1})/2$ ($\hat{\rho} = 2\sigma_\rho \xi_1$, $\hat{K}^{-1} = 2\sigma_K \xi_2$ for our models I and II), and

$$p = \frac{1}{2}[A\exp(i\omega z) + B\exp(-i\omega z)] , \tag{65b}$$

$$w = \frac{1}{2}[A\exp(i\omega z) - B\exp(-i\omega z)] . \tag{65c}$$

The variables in Eq. (65) are all expressed in terms of the natural units of the problem: $p \to p/K_0$, $w \to w/v_0$, $z \to z/\bar{a}$, $\omega \to \omega\bar{a}/v_0$. From Eq. (65a) it is easy to show that if one defines $R = B/A$, then R satisfies a Riccati equation[5]

$$\frac{dR}{dz} = i\omega[h\exp(2i\omega z) - 2gR + hR^2\exp(-2i\omega z)] . \tag{66}$$

For a finite slab of length L, we have $R(L) = 0$ because of the radiation boundary condition at the end of the slab, and Eq. (66) is to be integrated backward to the front interface $z = 0$, where R may be identified as the reflection coefficient. As $L \to \infty$, the boundary condition at $z = L$ may be determined by noting first that $|R| = 1$ because of the localizing nature of the random medium, then writing $R = \exp(i\psi)$ everywhere to obtain a corresponding equation[5] for ψ:

$$\frac{d\psi}{dz} = 2\omega[h\cos(\psi - 2\omega z) - g] . \tag{67}$$

Instead of a boundary condition at $z = L$ we now take the statistically stationary solution to Eq. (67). In terms of ψ the function $U_1(\Delta_\omega, \omega)$ can be written as

$$U_1(\Delta_\omega, \omega) = \langle \exp[i(\psi_1 - \psi_2)] \rangle = \int_0^{2\pi} d\bar{\psi}\, P(\bar{\psi}) \exp(i\bar{\psi}) , \tag{68}$$

where ψ_1 corresponds to the phase angle at frequency $\omega - (\Delta_\omega/2)$ and ψ_2 corresponds to the phase angle at frequency $\omega+(\Delta_\omega/2)$, $\overline{\psi} = \psi_1 - \psi_2$, and $P(\overline{\psi})$ denotes the stationary distribution of $\overline{\psi}$.

Up to now we have assumed that the random medium is bordered by a homogeneous medium with $\rho = \rho_0$, $K = K_0$. It is equally possible to have the other case where the random medium interfaces with vacuum so that backscattered waves are totally returned into the random medium. Since $p = 0$ is now the boundary condition at the interface for all times except during the application of the pressure pulse, one has to monitor the medium response in terms of the displacement velocity w at $z = 0$. In this case the expression corresponding to $U_1(\Delta_\omega, \omega)$ would be

$$U_2(\Delta_\omega, \omega) = \left\langle w\left(\omega - \frac{\Delta_\omega}{2}\right) w^*\left(\omega + \frac{\Delta_\omega}{2}\right)\right\rangle , \tag{69a}$$

where

$$w(\omega) = \frac{1 - R(\omega)}{1 + R(\omega)} . \tag{69b}$$

The particular form of w, Eq. (69b), may be deduced as follows. We write the pressure at $z = 0$ as a superposition of forward- and backward-going wave amplitudes in accordance with Eq. (65b):

$$p(\omega) = \frac{1}{2}(A + B) , \quad z = 0 .$$

If a $\delta(\tau)$ pulse is applied at $z = 0$, then $f(\omega) = 1$ for the pressure pulse and we have the condition of

$$\frac{A + B}{2} = 1 . \tag{70a}$$

The displacement velocity, in accordance with Eq. (65c), is given by

$$w = \frac{1}{2}(A - B) . \tag{70b}$$

By defining $R = B/A$ as a reflection coefficient and using Eq. (70a), we have $A = 2/(1 + R)$, $B = 2R/(1 + R)$, and

$$w = \frac{1 - R}{1 + R} . \tag{70c}$$

Since $R = \exp(i\psi)$, the right-hand side of Eq. (70c) can be singular. This ambiguity may be resolved by writing $R = r\exp(i\psi)$ in the definition of $U_2(\Delta_\omega,\omega)$ and let r approach unity from below. That is,

$$U_2(\Delta_\omega,\omega)$$
$$= \lim_{r_1,r_2\to 1^-}\left\langle\left[\frac{1-r_1\exp(i\psi_1)}{1+r_1\exp(i\psi_1)}\right]\left[\frac{1-r_2\exp(-i\psi_2)}{1+r_2\exp(-i\psi_2)}\right]\right\rangle$$

$$= \lim_{r_1,r_2\to 1^-}\left\langle\frac{1+r_1r_2\exp(i\bar{\psi})-\exp(i\bar{\psi}/2)[r_1\exp(i\psi_0)+r_2\exp(-i\psi_0)]}{1+r_1r_2\exp(i\bar{\psi})+\exp(i\bar{\psi}/2)[r_1\exp(i\psi_0)+r_2\exp(-i\psi_0)]}\right\rangle, \tag{71a}$$

where $\psi_0 = (\psi_1+\psi_2)/2$. The distribution of ψ_0 is expected to be uniform (this will be justified later) and therefore in the evaluation of U_2 we can first integrate ψ_0 from 0 to 2π with $P(\psi_0) = (2\pi)^{-1}$. A contour integration (with $\exp(i\psi_0)$ being the complex variable) yields

$$U_2(\Delta_\omega,\omega) = \lim_{r\to 1^-}\int_0^{2\pi}\frac{1+3r\exp(i\bar{\psi})}{1-r\exp(i\bar{\psi})}P(\bar{\psi})\,d\bar{\psi}\,, \tag{71b}$$

where $r = r_1r_2$. From $U_2(\Delta_\omega,\omega)$ the noise spectrum $N(\tau,\omega)$ may be obtained from Eq. (64b) with U_2 replacing U_1.

Equations (68) and (71b) tell us that the knowledge of $P(\bar{\psi})$ is necessary and sufficient for the evaluation of $U_{1,2}(\Delta_\omega,\omega)$ and $N(\tau,\omega)$ under both types of interface boundary conditions. To make further progress, we must derive the relevant stochastic differential equation for $P(\bar{\psi})$ and obtain its solution. The description of these tasks is presented in the next section.

5.2. Solution in the White Noise Limit

Up to now no approximation has been made in the derivation of the equations for R (Eq. (66)) and ψ (Eq. (67)). While the general solution of $P(\bar{\psi})$ based on these equations is not known, in this section we wish to show that the problem is analytically soluble in the white noise limit[5] of $\bar{a}\to 0$. More precisely, the limit involves the introduction of a dimensionless parameter $\bar{a}\omega/v_0 = \varepsilon \ll 1$ (not to be confused

with the dielectric constant symbol ε used in other sections) and the specification that $\bar{a}$ is on the order of ε^2 when measured in terms of a macroscale, taken to be 1. Physically, the macroscale may be thought of as the distance traveled by the pulse front during the time scale of non-stationarity $(\Delta\omega)^{-1}$ that we discussed before. The intermediate scale, v_0/ω, may be identified as the pulse width. This can be seen from the fact that since $\bar{a}/1 \sim \varepsilon^2$ and $\bar{a}\omega/v_0 = \varepsilon$, we must have $\omega \to \omega/\varepsilon$ so that the wavelength is on the order of $v_0/(\omega/\varepsilon) \sim \varepsilon$. On the other hand, Δ_ω is the difference frequency which determines the time scale for the non-stationarity and therefore $\Delta_\omega \to \Delta_\omega$ under the scale transformation. From Eq. (67), we can write a set of equations for ψ_1 and ψ_2 under the new scales:

$$\frac{d\psi_1^\varepsilon}{dz} = \frac{2\omega}{\varepsilon}\left[h^\varepsilon \cos\left(\psi_1^\varepsilon - 2\omega\frac{z}{\varepsilon} + \Delta_\omega z\right) - g^\varepsilon\right] - \Delta_\omega\left[h^\varepsilon \cos\left(\psi_1^\varepsilon - 2\omega\frac{z}{\varepsilon} + \Delta_\omega z\right) - g^\varepsilon\right], \tag{72a}$$

$$\frac{d\psi_2^\omega}{dz} = \frac{2\omega}{\varepsilon}\left[h^\varepsilon \cos\left(\psi_2^\varepsilon - 2\omega\frac{z}{\varepsilon} - \Delta_\omega z\right) - g^\varepsilon\right] + \Delta_\omega\left[h^\varepsilon \cos\left(\psi_2^\varepsilon - 2\omega\frac{z}{\varepsilon} - \Delta_\omega z\right) - g^\varepsilon\right]. \tag{72b}$$

Here we have assumed that random material fluctuations are generated by the random process $\boldsymbol{\xi}$ so that, $h^\varepsilon, g^\varepsilon$ can be written as $h^\varepsilon = h[\boldsymbol{\xi}(z/\varepsilon^2)]$, $g^\varepsilon = g[\boldsymbol{\xi}(z/\varepsilon^2)]$, i.e., material fluctuations occur on an extremely fast scale. What we want to examine is the effect of these fast material fluctuations integrated over the macroscale. Equation (72) can be written succinctly as

$$\frac{d\boldsymbol{\psi}^\varepsilon}{dz} = \frac{1}{\varepsilon}\mathbf{H}[z, \varsigma, \boldsymbol{\xi}, \Delta_\omega] + \mathbf{G}[z, \varsigma, \boldsymbol{\xi}, \Delta_\omega], \tag{72c}$$

where $\boldsymbol{\psi}^\varepsilon = (\psi_1^\varepsilon, \psi_2^\varepsilon)$, $\varsigma = z/\varepsilon$, and

$$\mathbf{H} = 2\omega\begin{bmatrix} h[\boldsymbol{\xi}]\cos(\psi_1 - 2\omega\varsigma + \Delta_\omega z) - g[\boldsymbol{\xi}] \\ h[\boldsymbol{\xi}]\cos(\psi_2 - 2\omega\varsigma - \Delta_\omega z) - g[\boldsymbol{\xi}] \end{bmatrix}, \tag{72d}$$

$$\mathbf{G} = \Delta_\omega\begin{bmatrix} -h[\boldsymbol{\xi}]\cos(\psi_1 - 2\omega\varsigma + \Delta_\omega z) + g[\boldsymbol{\xi}] \\ h[\boldsymbol{\xi}]\cos(\psi_2 - 2\omega\varsigma - \Delta_\omega z) - g[\boldsymbol{\xi}] \end{bmatrix}. \tag{72e}$$

The process $(\boldsymbol{\xi}, \boldsymbol{\psi}^\epsilon)$ is jointly Markovian with the infinitesimal generator

$$L^\epsilon = \frac{1}{\epsilon^2} Q + \frac{\partial \boldsymbol{\psi}^\epsilon}{\partial z} \cdot \boldsymbol{\nabla}_\psi$$
$$= \frac{1}{\epsilon^2} Q + \frac{1}{\epsilon} \mathbf{H} \cdot \boldsymbol{\nabla}_\psi + \mathbf{G} \cdot \boldsymbol{\nabla}_\psi \ . \tag{73}$$

From L^ϵ one can write the backward Kolmogorov equation

$$-\frac{\partial V^\epsilon}{\partial z} + \frac{1}{\epsilon^2} Q V^\epsilon + \frac{1}{\epsilon} \mathbf{H} \cdot \boldsymbol{\nabla}_\psi V^\epsilon + \mathbf{G} \cdot \boldsymbol{\nabla}_\psi V^\epsilon = 0 \tag{74a}$$

for any quantity $V^\epsilon(z, \boldsymbol{\xi}, \boldsymbol{\psi})$. We will consider the case where the conditions at $z = 0$ do not depend on $\boldsymbol{\xi}$ i.e.,

$$V^\epsilon(z, \boldsymbol{\xi}, \boldsymbol{\psi})|_{z=0} = V_0(\boldsymbol{\psi}) \ . \tag{74b}$$

To obtain the infinitesimal generator in the limit of $\epsilon \to 0$, let us expand Eq. (74a) in multiple scales of z and $\varsigma = z/\epsilon$ so that $\partial/\partial z \to \partial/\partial z + \epsilon^{-1} \partial/\partial \varsigma$. Then Eq. (74a) becomes

$$\frac{1}{\epsilon^2} Q V^\epsilon + \frac{1}{\epsilon} \left[\mathbf{H} \cdot \boldsymbol{\nabla}_\psi V^\epsilon - \frac{\partial V^\epsilon}{\partial \varsigma} \right] + \left[\mathbf{G} \cdot \boldsymbol{\nabla}_\psi V^\epsilon - \frac{\partial V^\epsilon}{\partial z} \right] = 0 \ . \tag{74c}$$

If z is measured on the macroscale, then ς is measured on the pulse-width scale. By expressing V^ϵ as

$$V^\epsilon = V^{(0)} + \epsilon V^{(1)} + \epsilon^2 V^{(2)} + \dots \ , \tag{75}$$

in Eq. (74c) and equating terms with the same powers of ϵ that results, we get

$$Q V^{(0)} = 0 \ , \tag{76a}$$

$$Q V^{(1)} + \mathbf{H} \cdot \boldsymbol{\nabla}_\psi V^{(0)} - \frac{\partial V^{(0)}}{\partial \varsigma} = 0 \ , \tag{76b}$$

$$Q V^{(n)} + \mathbf{H} \cdot \boldsymbol{\nabla}_\psi V^{(n-1)} - \frac{\partial V^{(n-1)}}{\partial \varsigma}$$
$$+ \mathbf{G} \cdot \boldsymbol{\nabla}_\psi V^{(n-2)} - \frac{\partial V^{(n-2)}}{\partial z} = 0 \ , n \geq 2 \ . \tag{76c}$$

The first equation tells us that $V^{(0)}$ is independent of $\boldsymbol{\xi}$, i.e. $V^{(0)} = V^{(0)}(z, \boldsymbol{\psi})$. Now multiplying Eq. (76b) by $\overline{P}(\boldsymbol{\xi})$, the stationary distribution of $\boldsymbol{\xi}$, and integrating with respect to $\boldsymbol{\xi}$ gives

$$0 = \int d\boldsymbol{\xi}\, \overline{P}(\boldsymbol{\xi}) Q V^{(1)} + \int d\boldsymbol{\xi}\, \overline{P}(\boldsymbol{\xi}) \mathbf{H} \cdot \boldsymbol{\nabla}_{\psi} V^{(0)} + \frac{\partial V^{(0)}}{\partial \varsigma}$$

$$= \int d\boldsymbol{\xi}\, V^{(1)} Q^{*} \overline{P}(\boldsymbol{\xi}) + \frac{\partial V^{(0)}}{\partial \varsigma} = \frac{\partial V^{(0)}}{\partial \varsigma} , \tag{77a}$$

where we recognize that since $\mathbf{H}$ (and $\mathbf{G}$ as well) is linearly proportional to ξ_1 and ξ_2 (h, g are functions of the fluctuating parts of ρ and K^{-1}, see Eq. (65a)), its average must be 0. Also $Q^{*}\overline{P}(\boldsymbol{\xi}) = 0$ (see Secs. 4.1 and 4.2). From Eq. (77a) and Eq. (76b) we get

$$V^{(1)} = -Q^{-1} \mathbf{H} \cdot \boldsymbol{\nabla} V_{\psi}^{(0)} + V_0^{(1)} . \tag{77b}$$

Since Q has a nontrivial null space as demonstrated by Eq. (76a), its inverse Q^{-1} must be defined in the sense of Eq. (29) and acts only on states that are perpendicular to the null space. The term $V_0^{(1)}$, on the other hand, is independent of $\boldsymbol{\xi}$ and lies in the null space of Q. Now the substitution of Eq. (77b) into Eq. (76c) with $n = 2$ yields

$$Q V^{(2)} - \mathbf{H} \cdot \boldsymbol{\nabla}_{\psi} Q^{-1} \mathbf{H} \cdot \boldsymbol{\nabla}_{\psi} V^{(0)} + \mathbf{H} \cdot \boldsymbol{\nabla}_{\psi} V_0^{(1)} - \frac{\partial V_0^{(1)}}{\partial \varsigma}$$

$$+ \mathbf{G} \cdot \boldsymbol{\nabla}_{\psi} V^{(0)} - \frac{\partial V^{(0)}}{\partial z} = 0 . \tag{78a}$$

By multiplying by $\overline{P}(\boldsymbol{\xi})$ and integrating with respect to $\boldsymbol{\xi}$, the terms $QV^{(2)}$, $\mathbf{H} \cdot \boldsymbol{\nabla}_{\psi} V_0^{(1)}$, and $\mathbf{G} \cdot \boldsymbol{\nabla}_{\psi} V^{(0)}$ in Eq. (78a) all vanish, giving

$$\frac{\partial V^{(0)}}{\partial z} + \frac{\partial V_0^{(1)}}{\partial \varsigma} + E[\mathbf{H} \cdot \boldsymbol{\nabla}_{\psi} Q^{-1} \mathbf{H} \cdot \boldsymbol{\nabla}_{\psi}]_{\boldsymbol{\xi}} V^{(0)} = 0 , \tag{78b}$$

where the notation $E[\ ]_{\boldsymbol{\xi}}$ is used to denote taking the expectation value with respect to $\boldsymbol{\xi}$, which is essentially averages over the material fluctuations on the ϵ^2 scale. We want to further average over the ε scale by applying the operation

$$E[\ ]_{\varsigma} = \lim_{T \to \infty} \frac{1}{T} \int_0^T d\varsigma .$$

The term $\partial V_0^{(1)}/d\zeta$ in Eq. (78b) would become $\lim_{T\to\infty}[V_0^{(1)}(\zeta = T) - V_0^{(1)}(\zeta = 0)]/T$ under the ζ averaging. If $V_0^{(1)}$ is bounded as $T \to \infty$, then the $V_0^{(1)}$ term vanishes, giving us the final result

$$\begin{aligned}
&\frac{\partial V^{(0)}}{\partial z} + E[\mathbf{H}\cdot\boldsymbol{\nabla}_\psi Q^{-1}\mathbf{H}\cdot\boldsymbol{\nabla}_\psi]_{\epsilon,\zeta}V^{(0)} \\
&= \frac{\partial V^{(0)}}{\partial z} - \int_0^\infty ds\, E[\mathbf{H}[z,\boldsymbol{\xi}(0)]\cdot\boldsymbol{\nabla}_\psi\mathbf{H}[z,\boldsymbol{\xi}(s)]\cdot\boldsymbol{\nabla}_\psi]_{\epsilon,\zeta}V^{(0)} \\
&= 0\,,
\end{aligned} \tag{78c}$$

where we have used Eq. (29) as the definition of Q^{-1}. It is immediately recognized that Eq. (78c) is exactly the backward Kolmogorov equation in the limit of $\varepsilon \to 0$ since now ϵ has disappeared during the averaging process. The limiting infinitesimal generator is seen to be

$$L = \int_0^\infty ds\, E[\mathbf{H}[z,\boldsymbol{\xi}(0)]\cdot\boldsymbol{\nabla}_\psi\mathbf{H}[z,\boldsymbol{\xi}(s)]\cdot\boldsymbol{\nabla}_\psi]_{\epsilon,\zeta}\,. \tag{79}$$

By using the fact that

$$\boldsymbol{\nabla}_\psi\mathbf{H}\cdot\boldsymbol{\nabla}_\psi = (\mathbf{H}\cdot\boldsymbol{\nabla}_\psi)\boldsymbol{\nabla}_\psi + (\boldsymbol{\nabla}_\psi\mathbf{H})\cdot\boldsymbol{\nabla}_\psi\,, \tag{80}$$

and that the ζ averaging yields a factor of $1/2$ for the square of the cosine terms, $\cos(\psi_1 - \psi_2 + 2\Delta_\omega z)/2$ for the cross-cosine terms, and zero for everything else, the operator L may be evaluated explicitly as

$$\begin{aligned}
L = 4\omega^2\Big\{&\alpha_{gg}\Big[\frac{\partial}{\partial\psi_1} + \frac{\partial}{\partial\psi_2}\Big]^2 + \frac{1}{2}\alpha_{hh}\Big[\frac{\partial^2}{\partial\psi_1^2} + \frac{\partial^2}{\partial\psi_2^2} \\
&+ 2\cos(\psi_1 - \psi_2 + 2\Delta_\omega z)\frac{\partial^2}{\partial\psi_1\partial\psi_2}\Big]\Big\}\,,
\end{aligned} \tag{81a}$$

where

$$\alpha_{gg} = \int_0^\infty ds\langle g(0)g(s)\rangle\,, \tag{81b}$$

and

$$\alpha_{hh} = \int_0^\infty ds\langle h(0)h(s)\rangle \tag{81c}$$

are the integrals of the correlation functions for g and h. Here we have used the notations $g(s) = g[\xi(s)]$, $h(s) = h[\xi(s)]$, and $\langle\ \rangle$ for $E[\ ]_\ell$ (same as configurational averaging because of ergodicity). From the definition of g and h as $(\hat{\rho} \pm \hat{K}^{-1})/2$ and comparison with Eq. (32), we immediately obtain the equivalence of $\alpha_{gg} = (\alpha_{\rho\rho} + \alpha_{KK} + 2\alpha_{\rho K})/4$ and $\alpha_{hh} = (\alpha_{\rho\rho} + \alpha_{KK} - 2\alpha_{\rho K})/4$. Furthermore, the low-frequency localization length is simply given by

$$l(\omega) = \frac{v_0^2}{\alpha_{hh}\omega^2}\,, \quad \omega \to 0 \tag{82}$$

as indicated by Eq. (34b).

From Eq. (81) we can now get L in terms of $\overline{\psi} = \psi_1 - \psi_2$ and $\psi_0 = (\psi_1 + \psi_2)/2$:

$$L = 4\omega^2 \left\{ \left(\alpha_{gg} + \frac{1}{4}\alpha_{hh}[1 + \cos(\overline{\psi} + 2\Delta_\omega z)] \right) \frac{\partial^2}{\partial \psi_0^2} + \alpha_{hh}[1 - \cos(\overline{\psi} + 2\Delta_\omega z)] \frac{\partial^2}{\partial \overline{\psi}^2} \right\}\,. \tag{83}$$

Note that the coefficients in Eq. (83) do not depend on ψ_0. That means the knowledge of $\overline{\psi}$ at any position z is sufficient to predict the state at $z + dz$, i.e. $\overline{\psi}$ is Markovian by itself. For ψ_0, on the other hand, the only stationary distribution form compatible with Eq. (83) would be $a\psi_0 + b$. Since on physical basis there is no reason to expect $-\psi$ to be any different from $+\psi$, we conclude that $P(\psi_0)$ must be uniform as asserted earlier. By taking into account these considerations, the Fokker-Planck equation $L^* P = \partial P/\partial z$ for the distribution $P(\overline{\psi})$ may be written in the following form:

$$4\omega^2 \alpha_{hh} \frac{\partial^2}{\partial \overline{\psi}^2}[1 - \cos(\overline{\psi} + 2\Delta_\omega z)]P = \frac{\partial P}{\partial z}\,. \tag{84a}$$

By making a variable transformation $\overline{\psi} + 2\Delta_\omega z \to \overline{\psi}'$, $z \to z'$, we get $\partial/\partial z' \to \partial/\partial z' + (\partial\overline{\psi}'/\partial z')(\partial/\partial\overline{\psi}') = \partial/\partial z' + 2\Delta_\omega \partial/\partial\overline{\psi}'$ so that

$$\frac{\partial P}{\partial z} + 2\Delta_\omega \frac{\partial P}{\partial \overline{\psi}} = 4\omega^2 \alpha_{hh} \frac{\partial^2}{\partial \overline{\psi}^2}[1 - \cos\overline{\psi}]P\,, \tag{84b}$$

where we have dropped the primes. In the new equation the argument of the cosine is no longer dependent on z. For stationary distribution, we may set $\partial P/\partial z = 0$ to get

$$\Delta_\omega \frac{\partial}{\partial s}(1+s^2)P(s) + 2\omega^2\alpha_{hh}\frac{\partial}{\partial s}(1+s^2)\frac{\partial P(s)}{\partial s} = 0\,, \qquad (85)$$

where $s = \cot(\bar{\psi}/2)$ so that $\partial/\partial\bar{\psi} = -[(1+s)^2/2]\partial/\partial s$, $1-\cos\bar{\psi} = 2/(1+s^2)$, and $P(\bar{\psi}) = P(s)(\partial s/\partial\bar{\psi}) = -(1+s)^2P(s)/2$. Equation (85) may be solved by quadrature[5]:

$$P_{\Delta_\omega}(s) = \frac{\Delta_\omega}{2\pi\omega^2\alpha_{hh}}\int_0^\infty \frac{\exp\left(-\Delta_\omega q/2\omega^2\alpha_{hh}\right)}{1+(q-s)^2}\,dq\,, \quad \Delta_\omega \geq 0\,. \qquad (86a)$$

If $\Delta_\omega < 0$, the change of $s \to -s$ in Eq. (85) is seen to take the equation back to its original state. Therefore,

$$P_{-\Delta_\omega}(s) = P_{\Delta_\omega}(-s)\,. \qquad (86b)$$

To evaluate $U_1(\Delta_\omega,\omega)$, we simply recognize that $\exp(i\bar{\psi}) = (s+i)/(s-i)$. For the matched-medium boundary condition that means

$$\begin{aligned} U_1(\Delta_\omega,\omega) &= \int_{-\infty}^{\infty} P_{\Delta_\omega}(s)\ \frac{s+i}{s-i}ds = U_1(y) \\ &= y\int_0^\infty \exp(-qy)\frac{q}{q+i}dq\,, \quad y>0 \end{aligned} \qquad (87)$$

and $U_1^*(-y) = U_1(y)$. Here $y = \Delta_\omega l(\omega)/v_0$, with $l(\omega)$ expressing the low-frequency localization length as given by Eq. (82).

The fact that U_1 is a function of only one variable y has the following physical implications. In the last section we have predicted that the function $U_1(\Delta_\omega,\omega)$ must decay to zero over a finite width $|\Delta_\omega| < \Delta\omega$, where $(\Delta\omega)^{-1}$ gives the time scale of non-stationary for the multiple scattering noise. Numerical evaluation of Eq. (87) (see Fig. 9 in next section) now indeed tells us that $U_1(y)$ has a width of $\Delta y \simeq 1$. From the definition of $y = \Delta_\omega l(\omega)/v_0$, we get

$$(\Delta\omega)^{-1} \simeq \frac{l(\omega)}{v_0}\,. \qquad (88)$$

That is, the width of the function U_1 scales as $l^{-1}(\omega)$, and therefore the time scale of non-stationarity is directly proportional to $l(\omega)$. Since $l(\omega)$ increases as ω decreases, it follows that the low-frequency components of the multiple scattering noise should persist longer than the high-frequency components. This is intuitively reasonable because the high-frequency components of the pulse should be reflected into the homogeneous medium much earlier due to the shorter localization length. This phenomenon may indeed be detected by looking at numerically simulated coda as shown in Fig. 1.

For the case of totally-reflecting boundary condition at the interface, the injected pulse energy would be trapped by a reflecting boundary on the one end and by a nonpenetrable random medium on the other. The noise statistics is therefore expected to be stationary. The evaluation of $U_2(\Delta_\omega, \omega)$ means the calculation of the following integral:

$$\begin{aligned} U_2(\Delta_\omega, \omega) &= \lim_{r \to 1^-} \int_{-\infty}^{\infty} P_{\Delta_\omega}(s) \left[\frac{(3r+1)s + i(3r-1)}{(1-r)s - i(1+r)} \right] ds \\ &= \lim_{r \to 1^-} \int_{-\infty}^{\infty} dq \, \frac{y \exp(-yq/2)}{2\pi} \\ &\quad \times \int_{-\infty}^{\infty} ds \, \frac{[(3r+1)s + i(3r-1)]}{[1+(q-s)^2][(1-r)s - i(1+r)]} \\ &= 1 - i\frac{4}{y} \\ &= U_2(y) \, . \end{aligned} \tag{89}$$

The noise spectrum $N(\tau, \omega)$ can now be obtained directly from U_1 and U_2 by a Fourier transform:

$$N(\tau, \omega) = \frac{\chi}{2\pi\tau} \int_{-\infty}^{\infty} dy \exp(-iy\chi) U_{1,2}(y)$$

$$= \begin{cases} \dfrac{1}{\tau}\mu_1(\chi); & \text{matched-medium B.C.} \\ \\ \dfrac{v_0}{l(\omega)}\delta(\chi) + \dfrac{1}{\tau}\mu_2(\chi); & \text{reflecting B.C.} \, , \end{cases} \tag{90a}$$

where

$$\mu_1(\chi) = \frac{\chi}{(1+\chi)^2} H(\chi) \ , \tag{90b}$$

$$\mu_2(\chi) = 4\chi H(\chi) \ , \tag{90c}$$

$$\chi = \frac{\tau v_0}{l(\omega)} \ . \tag{90d}$$

Here $H(\chi)$ is the unit step function defined as $H(\chi) = 1$ for $\chi \geq 0$ and $H(\chi) = 0$ for $\chi < 0$. It is clear that the scaling in the Δ_ω domain naturally implies scaling in the τ domain through the definition of the variable χ. While the forms and the physical implications of $\mu_1(\chi)$ and $\mu_2(\chi)$ will be discussed in Sec. 5.4., we just wish to note here that for μ_1, the condition of $U_1(y = 0) = 1$ implies a sum rule for μ_1 in the form of

$$U_1(0) = \int_{-\infty}^{\infty} \chi^{-1} \mu_1(\chi) d\chi = 1 \ . \tag{91}$$

From the form of $\mu_1(\chi)$, Eq. (90b), this is indeed true. For $\mu_2(\chi)$, no such sum rule exists, but at $\tau > 0$, $N(\tau, \omega) = 4\chi/\tau = 4v_0/l(\omega)$ is independent of τ as expected.

5.3. Numerical Simulations

Since the analytical results obtained in the last section are based on the assumption of $\bar{a}\omega/v_0 = \varepsilon \to 0$, a natural use of numerical simulations would be to examine the prediction of the theory when the ratio $\bar{a}\omega/v_0$ is no longer small. What we find is that the theory is surprisingly accurate for all ranges of the ratio $\bar{a}\omega/v_0$ provided one uses not just the low frequency expression for $l(\omega)$ but the true value of $l(\omega)$ when ω is beyond the low frequency regime. This indicates to us that the analytical results have general validity.

To compare our analytical results with numerical simulation data which can extend beyond the white-noise limit, we choose to focus only on the set $U_1(y)$ and $\mu_1(\chi)$ since the same basic quantity $P(\overline{\psi})$ is used

to evaluate both U_1 and U_2. To obtain $U_1(y)$, we use the transfer-matrix algorithm as described in Sec. 4.5 to calculate $R_{1,2} = \exp(i\psi_{1,2})$. $U_1 = \langle \exp(i\overline{\psi}) \rangle$ is then obtained by configurational averaging. Care is taken in using sufficient large sample length L so that $|R| = 1$ and the value of $\overline{\psi}$ stabilizes. All three material models were simulated. For model I, we used $\bar{a} = 1$, $\rho_0 = 8$, $K_0 = 2$, $\sigma_\rho = 0.05$, and $\sigma_K = 0.4$. In model II the parameters are $\bar{a} = 1$, $\rho_0 = K_0 = 1$, $\sigma_\rho = 0.9$, and $\sigma_K = 0.9$. For model III we just get the material parameters from model II by convolving with an exponential filter. For a particular value of ω in a given model, U_1 is calculated as a function of Δ_ω. A total of 32 curves is obtained with frequencies ranging from $\bar{a}\omega/v_0 \sim 0.05$ to $\bar{a}\omega/v_0 \sim 10$. When $\mathrm{Re}(U_1)$ and $\mathrm{Im}(U_1)$ are plotted as a function of $\ln \Delta_\omega$, all the curves appear to be similar except that they are horizontally displaced from one another. This suggests the introduction of a scaling frequency $\Delta_s = v_0/l_s$ for each curve whose role is to scale Δ_ω such that when the curves are plotted as $\ln(\Delta_\omega/\Delta_s) = \ln(\Delta_\omega l_s/v_0)$ all the data would collapse into a single functional form. The value of $l_s(\omega)$ obtained in this way can then be compared with independently calculated localization length $l(\omega)$ to see if $y = \Delta_\omega l(\omega)/v_0$ is indeed the scaling variable. In Fig. 9 we compare the collapsed simulation data with the prediction of the theory as evaluated from Eq. (87). The good agreement of the different curves with each other and with the theory indicates that U_1 is truly a function of only one variable, and in terms of this variable the functional form $U_1(y)$ is universal in the sense of being independent from model parameters and statistics. The function $U_1(y)$ is also noted to have a width of about $\Delta y \simeq 1$. In Fig. 10 we compare the values of $l_s(\omega)$ with that of numerically evaluated $l(\omega)$. For clarity, only those data for models I and II are shown. The remarkable tracking of $l_s(\omega)$ with $l(\omega)$ leaves no doubt that $l_s(\omega)$ is in fact the localization length (data for model III show equally good tracking). Also, the frequency range over which the scaling holds is seen to be very large. We therefore conclude that the ω-dependence of the multiple scattering noise spectrum is completely determined by $l(\omega)$.

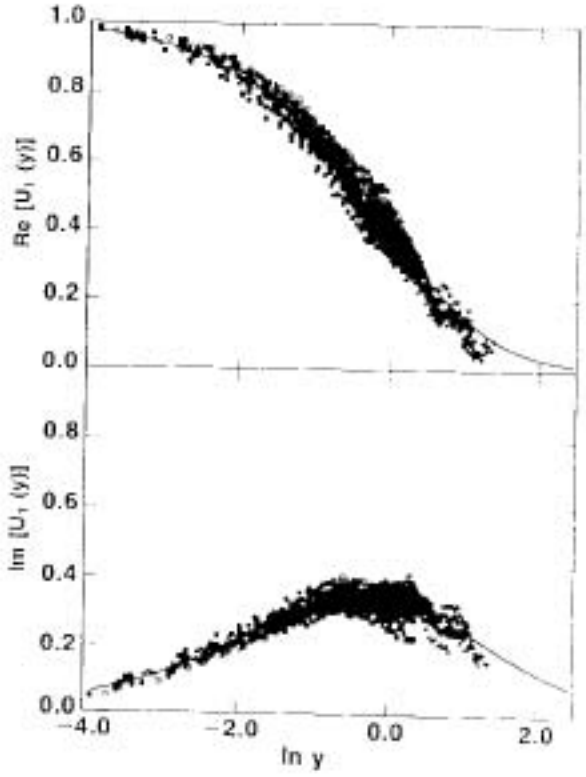

Fig. 9. The real and imaginary parts of $U_1(y)$ for the matched-medium case plotted as functions of ln y, where $y = \Delta_\omega l_s(\omega)/v_0$. Solid line denotes the prediction of the analytical theory as evaluated from Eq. (87). The symbols denote the simulation results for a total of 32 cases involving the three models and different values of the frequency ω. Each symbol represents the average of over 40 configurations.

In the time domain, we simulate $\mu_1(\chi)$ directly by solving the wave equation

$$K^{-1}(z)\frac{\partial^2 p}{\partial t^2} = \frac{\partial}{\partial z}\rho^{-1}(z)\frac{\partial p}{\partial z}$$

numerically for 900 configurations of model I with a Gaussian incident pulse. By Fourier transformation of $\langle p(\tau)p(\tau+t)\rangle$ with respect to t, we get $S(\tau,\omega)$ for five different observation window times τ. The values of $\mu_1(\chi)$ shown in Fig. 11 are evaluated as $S(\tau,\omega)\tau/|f(\omega)|^2$ and plotted as a function of $\sqrt{\chi}$ by using the numerically calculated values of the localization length. We use $\sqrt{\chi}$ as the plotting variable because at low frequencies $\sqrt{\chi}\,\alpha\,\omega$, which makes the plotted curve proportional to the noise spectrum in that limit. It is seen that the scaling property of $\mu_1(\chi)$ is indeed verified in that the data for different windows collapse

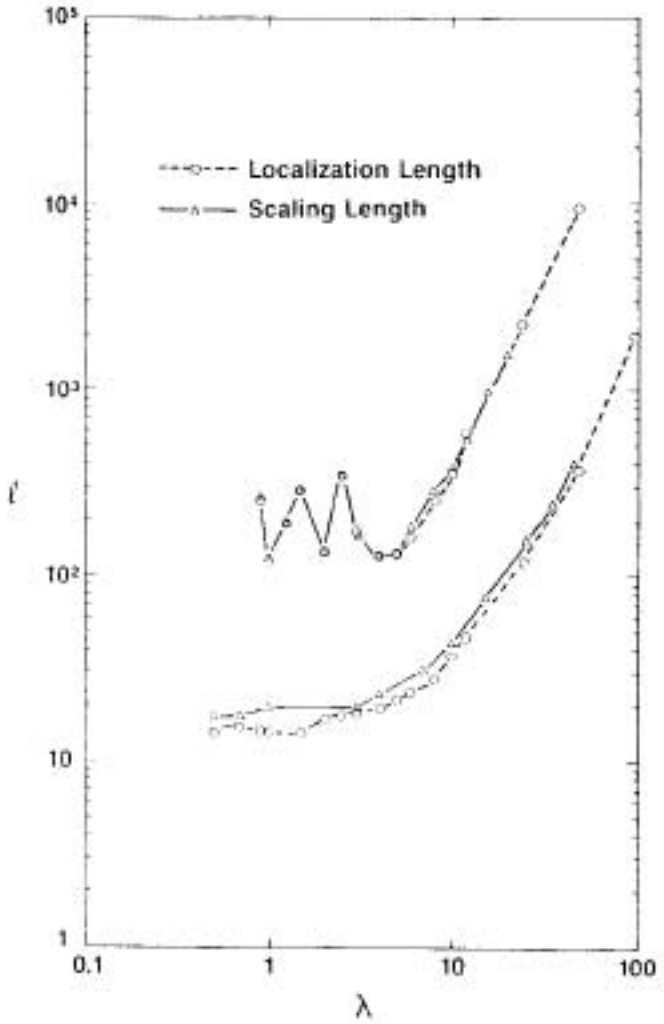

Fig. 10. The comparison between the scaling length obtained by collapsing the data in Fig. 9, and the independently calculated localization length. Both are in units of mean layer thickness $\bar{a}$. Results for model I are shown in the upper pair of curves, and those for model II are shown in the lower pair.

into a single curve when plotted in terms of the variable χ. Comparison with the theoretical prediction also shows obvious agreement, although the numerical peak value at $\chi = 1$ is higher than predicted. This could be due to numerical inaccuracies arising from fluctuations in the data, which are largest near $\chi = 1$.

The excellent agreement between the simulation data and the analytical results does raise an interesting question. While the independence of $U_{1,2}(y)$ from the different types of model and model parameters is implicit in our derivation and therefore understandable, yet why

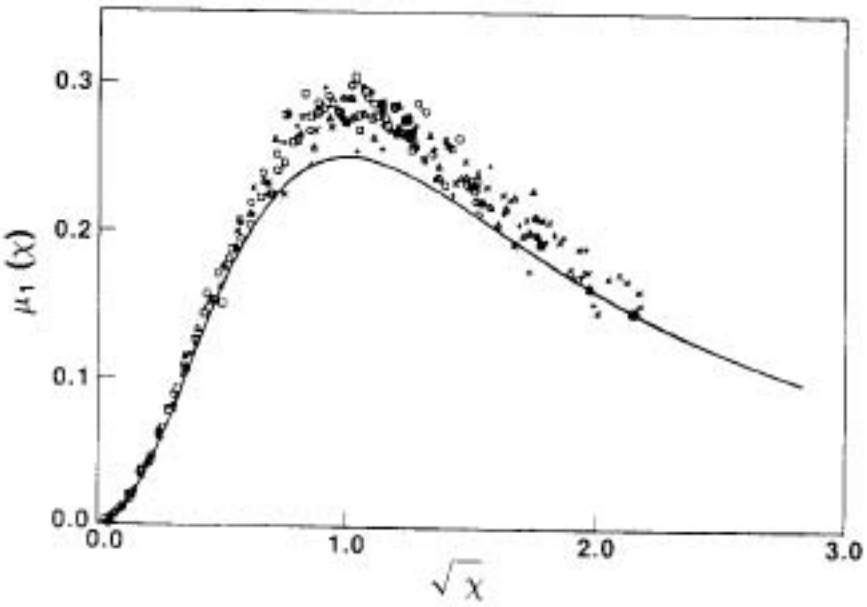

Fig. 11. The noise spectrum $\mu_1(\chi)$ plotted as a function of $\sqrt{\chi}$ where $\chi = \tau v_0/l(\omega)$. The simulation data, denoted by symbols, are obtained by solving the wave equation in the time domain for model I. In time units of $\bar{a}/v_0$, scaled noise data for $\tau = 200$, 300, 400, 500 and 600 are shown. Solid line is the curve $\chi/(1+\chi)^2$.

should the results of the theory be valid at all frequency ranges when their derivation is based on the low-frequency assumption? We speculate that perhaps the present results are derivable from a much more general set of assumptions. One plausible general criterion for the validity of the theory is that the dimensionless parameter $Q^{-1} = 2v_0/\omega l(\omega)$ be small, where Q is usually denoted as the "quality factor". Since we have seen that $l(\omega)$ is always bounded below by a fairly large minimum value (see Sec. 4.5) even for a medium with very large material parameter fluctuations, Q^{-1} would therefore have a maximum value that is $\ll 1$ for all frequencies. Physically, that means the multiple-scattering attenuation is always a weak effect over a pulse-width. If that is the case, then $\omega\bar{a}/v_0 = \varepsilon \ll 1$ is just one realization of the general criterion and therefore would be a sufficient, but not necessary, condition for the derivation of the analytical results. In any case, our simulation data clearly demonstrate the general applicability of the analytical results.

5.4. Physical Implications

Knowledge of the form for $\mu_{1,2}(\chi)$ has direct implications for the measurement of the localization length in the time domain.[5] In the case of matched-medium boundary condition, it indicates that on measuring $\tau N(\tau,\omega) = \mu_1(\chi)$ at a certain frequency window, one should observe a peak at some time τ_0 (with the time of pulse injection taken to be $\tau = 0$) corresponding to $\chi = \tau_0 \cdot v_0/l(\omega) = 1$. Thus, knowing the mean speed of the random medium would yield $l(\omega) = \tau_0 v_0$. If v_0 is not known, one can still get a relative ratio of the localization lengths for different random media by comparing the peaking times. For the pressure-release boundary conditions, on the other hand, $N(\tau,\omega) = 4v_0/l(\omega)$ so that the localization length is proportional to the inverse of the noise spectrum and therefore can again be determined directly in the time domain.

A curious feature about $\mu_1(\chi)$ is that it has a universal maximum value of $1/4$. That means the maximum $\tau N(\tau,\omega)$ value for all randomly stratified media should be the same, regardless of the magnitude of the material-parameter fluctuations. This is somewhat anti-intuitive at first sight because one would normally expect the medium with large-magnitude fluctuations in ρ or K^{-1} to be strongly scattering and therefore to yield a higher magnitude for the maximum of μ_1. But in reality what happens, as evidenced by our analytical and numerical results, is that for different media only the peaking times of $\tau N(\tau,\omega)$ are different. For a medium with small randomness one has to wait longer before the same peak magnitude of $\tau N(\tau,\omega)$ is achieved.

The validity of our analytical results for the pulse reflection problem for all values of ω means that if $l(\omega)$ is known, then $N(\tau,\omega)$ may be explicitly predicted. In the case of a model-II type medium, for example, we have $l(\omega) \cong c_1^{-1} + 6v_0^2/(\sigma^2\omega^2 a)$ (where $\sigma = \sigma_\rho = \sigma_K$) as an accurate representation for $l(\omega)$ over the entire frequency range. That means

$$N(\tau,\omega) = \begin{cases} \dfrac{c_1^{-1} + \frac{6}{a}(\frac{v_0}{\sigma\omega})^2}{[c_1^{-1} + \frac{6}{a}(\frac{v_0}{\sigma\omega})^2 + \tau v_0]^2}\, v_0\,, & \text{matched-medium} \\ \\ [c_1^{-1} + \dfrac{6}{a}(\dfrac{v_0}{\sigma\omega})^2]^{-1}\, v_0\,, & \text{reflecting}\,, \end{cases} \tag{92}$$

where c_1 can be calculated from Eq. (48). The knowledge of $N(\tau,\omega)$ may enable one to optimally detect reflections from target objects buried in a random medium. Of course, $N(\tau,\omega)$ represents only an expected value. Results of measurement from a single configuration are expected to show large fluctuations.

In this work we have not considered the parallel effect of dissipative attenuation. Of course, if the dissipative attenuation length $l_d(\omega)$ is significantly smaller than the localization length, then the attenuation effects of multiple scattering would obviously be secondary and we would not expect to observe true localization effects. On the hand, if the $l_d(\omega) > l(\omega)$, then we might view the dissipation and multiple scattering as two independent sources of attenuation, and in that case it can be shown that the power spectrum $\mu_{1,2}$ is multiplied by the factor $\exp(-2\gamma_0\tau/\rho_0)$, where $\gamma_0 = \langle\gamma_i\rangle$ and γ_i (displacement velocity) represents the local dissipation in ith layer.

6. CONCLUDING REMARKS

In this paper we have delineated in some detail the recent theoretical developments on the problem of wave propagation in randomly stratified media. While a fair amount is already known, yet much remains to be done. For the pulse scattering problem, for example, there is obviously a general theory waiting to be uncovered that would relax the low-frequency assumption. Challenges also exist in understanding the statistics of pulse transmission through a finite slab of random medium, as well as in the application of the present approach to the problem of statistical data inversion. By the latter we mean a generalization of the model so that the mean of the material parameters, ρ_0 and K_0, are no longer constant but can actually vary over distances that are large as compared with $\bar{a}$. The aim of an inversion scheme would then be the optimal recovery of $\rho_0(z)$ and $K_0(z)$ from noisy data, where the noise arises from multiple scattering by material fluctuations on the scale of $\bar{a}$.

On a more general level, one may consider a model where each layer may contain lateral inhomogeneities. By adjusting the amount of lateral fluctuations, it is possible to cross over from one-dimensional ran-

domness to fully three-dimensional randomness. The study of this more general model, however, would require mathematical methods very different from those considered here, and we leave it as a subject of future inquiry.

APPENDIX

THE TRACE THEOREM

For differential equations of the type

$$\frac{d}{dz}Y = tY \ , \tag{A.1}$$

where Y and t are $n \times n$ matrices, it is simple to show that there is a relationship between the determinant of Y and the trace of t. Equation (A.1) can be rewritten as

$$Y(z + \Delta z) = (1 + t\Delta z)Y(z) \ . \tag{A.2}$$

By taking the determinant of both sides, we get

$$\begin{aligned} \det(Y)_{z+\Delta z} &= \det(1 + t\Delta z)\det(Y)_z \\ &\cong [1 + \mathrm{Tr}(t)\Delta z]\det(Y)_z \end{aligned} \tag{A.3}$$

to the first order in Δz. That means

$$\frac{d}{dz}\det(Y) = \mathrm{Tr}(t)\det(Y) \ . \tag{A.4}$$

If $\mathrm{Tr}(t) = 0$ as in the case of Eq. (5), then $\det(Y)$ is a constant independent of z. That means if one set of solution, say (p_1, u_1), decays like $\exp(-\gamma z)$, then the second set of solution (p_2, u_2) must grow exponentially as $\exp(\gamma z)$ with exactly the same γ so that the determinant of the solution matrix would maintain its constancy as a function of z.

REFERENCES

1. See for example, K. Aki and P. G. Richards, *Quantitative Seismology* (W. H. Freeman, San Francisco, California, 1980).
2. See, for example, B. Souillard, "Waves and Electrons in Inhomogeneous Media" in *Chance and Matter*, J. Souletie, J. Vannimenus and R. Stora, eds. (North-Holland, Amsterdam, 1987), and references therein.
3. R. Burridge, G. Papanicolaou and B. White, *SIAM J. Appl. Math.* **47** (1987) 146.
4. P. Sheng, Z. Q. Zhang, B. White and G. Papanicolaou, *Phys. Rev. Lett.* **57** (1986) 1000.
5. B. White, P. Sheng, Z. Q. Zhang and G. Papanicolaou, *Phys. Rev. Lett.* **59** (1987) 1918.
6. P. Sheng, B. White, Z. Q. Zhang and G. Papanicolaou, *Phys. Rev.* **B34** (1986) 4757.
7. P. G. Richards and W. Menke, *Bull. of Seismological Soc. of Am.* **73** (1983) 1005.
8. W. Menke, *Geophys. J. Res. Astr. Soc.* **75** (1983) 541.
9. J. E. Sipe, P. Sheng, B. W. White and M. H. Cohen, *Phys. Rev. Lett.* **60** (1988) 108.
10. S. John, H. Sompolinsky and M. J. Stephen, *Phys. Rev.* **B27** (1983) 5592.
11. M. Y. Azbel, *Phys. Rev.* **B28** (1983) 4106.
12. W. Kohler and G. Papanicoloau, *J. Math. Phys.* **14** (1973) 1733.
13. M. Schoenberger and F. K. Levin, *Geophysics* **39** (1974) 278.
14. M. Schoenberger and F. K. Levin, *Geophysics* **43** (1978) 730.
15. R. F. O'Doherty and N. A. Anstey, *Geophysical Prospecting* **19** (1971) 430.
16. C. W. Gardiner, *Handbook of Stochastic Methods for Physics, Chemistry and the Natural Sciences* (Springer-Verlag, New York, 1983).
17. M. Born and E. Wolf, *Principle of Optics*, 2nd edn. (Pergamon Press, New York, 1964) p. 43.